8-2012

Deformation and Adhesion of Thin Metallic Films on Flexible Substrates

Julia Reid
Clemson University, julia@g.clemson.edu

DEFORMATION AND ADHESION OF THIN METALLIC FILMS ON FLEXIBLE SUBSTRATES

A Thesis
Presented to
the Graduate School of
Clemson University

In Partial Fulfillment
of the Requirements for the Degree
Master of Science
Materials Science and Engineering

By
Julia Reid
August 2012

Accepted by:
Dr. M. Kennedy, Committee Chair
Dr. J. Ballato
Dr. J. Luo

ABSTRACT

Flexible electronics are conductive circuits, components and lines integrated onto elastic substrates. These systems often consist of metallic thin films deposited onto thin sheets of glass, metals stainless steel or polymeric materials such as polyethylene or polystyrene. These systems are currently being studied for a wide variety of aeronautic and astronautical applications including: electronic skins, solar sails, and antennae structures. For applications include only moderately elevated temperatures (near 200 °C) and low strains (insert range), engineers have proposed incorporation metallic lines onto polymeric substrates. Like traditional microelectronic systems with films on hard substrates, the reliability is controlled by the film-substrate interfacial strength and film structure. Currently, there are no reliable models or experimental studies that examine how these if deformation in the substrate takes places. To design these models, experimental evidence of how these systems deform is needed. This project looks at adhesion energy as a function of thickness, rigid interlayer, and substrate stiffness and substrate deformation. This study will also examine bulge testing as a way to characterize flexible electronic systems and will be modified to be capable of testing with heat. This study has three major aims. The first was to characterize the fracture pathways and morphology from delamination due to compressive and tensile residual stress. The second aim was to differentiate between deformation seen in rigid substrates from that seen in compliant substrates. The last aim was to design a bulge test system that is capable of controlled strain rate and moderate temperature ranges.

This study looked at three distinct behaviors of metallic films on polymer substrates. The first part of this study looked at how film thickness, interlayer chemistry and thin film residual stress influence the fracture along the metal-polymer interface. This was done by observing fracture on two model systems, W/PMMA and W/PS. Tungsten was chosen since this films system can be deposited with a large rage stresses. Compressive and tensile W films (100-600nm) were sputter deposited onto PMMA and also PS substrates. The PS and PMMA systems were characterized using Hutchinson and Sou's models for rigid elastic systems.

For tensile driven fracture of the interface between W/PS it was found that as film thickness increases so does energy release rate (0.002 J/m^2 to 0.011 J/m^2) since the true adhesion does not change. With the inclusion of an interlayer the energy release rate decreased by an order of magnitude (.001 J/m^2 to 0.035 J/m^2). The compressive W/PMMA systems showed the same trends; an increase in energy release rate with an increase in film thickness; however, trends of varying buckle sized were observed on the 400 and 600 nm films. The compressive films without an interlayer were up to 3 orders of magnitude larger than the tensile films (0.8 J/m^2 to 2.4 J/m^2) and the interlayer only slightly increase the energy release rate (0.4 J/m^2 to 2.8 J/m^2). A "ridge" formation in the W/PMMA around the crack tip has been identified, this substrate deformation not seen in metal-ceramic systems. A large buckles corresponds to a large amount of deformation seen in the substrate, film thickness showed no apparent trend.

Bulge testing, is a testing method capable of characterize the composite modulus, residual stress, adhesion and other system properties of these flexible systems. The Clemson University system was verified for system repeatability.

The Clemson University bulge test system measures the deflection of membranes. Using a Polytec MSA 400 laser vibrometer, capable of taking submicron deflection measurements when pressure is applied using a, Druck DP515 pressure controller, which can control the strain rate (0.1 psi/s to 2 psi/s) and a maximum pressure of 30 psi and is accurate to 0.001 psi. The membrane geometry and diameter were either controlled by a Swagelok clamping system for roll-to-roll applications or micromachined membranes, fabricated at the University of Minnesota Nanotechnology Center. The clamping design allowed for use of 4 mm, 6mm and 10 mm diameter circular membranes. Additional considerations for improving the measurements of flexible systems were adjusting the clamping system design to include a microstage, data curve fitting and super gluing the sample to the clamp to provide accurate and reproducible measurements (that range from +/- 500 μm), using 100 nm Au on 25 μm of Kapton as a model system.

A heater was added to measure the effects of temperature on the deflection of flexible systems. Using ceramic heaters (maximium temperature of 300 °C) inserted into holes drilled in the side of the clamp, an Omega CNi1/8 temperature controller (accurate to 0.5 °C) was used to regulate the temperate with feed back from a J-type thermocouple. The system was verified using a one μm clamped in a six mm circular clamp and found a biaxial modulus of 150 GPa and residual stress of 180 MPa. However, the system showed that was susceptible to and external resonance frequency. This was done by

applying a load of three psi and holding for an interval lasting from ten minutes to one hour. The creep could not be calculated due to interference from an outside system, however the strain rates (from 0.1 PSI/s to 2.0 PSI/s) at lower temperature show no effect on the system. When the temperature was increased to 150 °C the higher strain rates showed more deflection. This was not expected because thinner polymer membranes have less strain rate sensitivity.

ACKNOWLEDGMENTS

I would like to thank my Mother, Father, little brothers (Daniel and Michael), and my amazing grandparents who all provided constant encouragement and perspective during the duration of my graduate studies.

In addition, I need to thank all my friends (near and far) who were there for me when I needed a shoulder to lean on and also provided constant support during my journey. Thank you.

An enormous thank you to my advisor, Dr. M. Kennedy, whose patience, understanding and guidance were immeasurable during my time at Clemson University. Thanks for not loosing faith in me.

Thanks to my advising committee members Dr. J. Luo and Dr. J. Ballato, who provided support and wisdom throughout my stay. Thanks to my group members, Ross Economy, Nathan Mitchell, and Gloria Chen, who helped me throughout this process and lead me to look at the bright side of things. Thank you to Dr. Daqaq and his group who patiently shared a lab. In addition, Dr. JoAn Hudson and her colleagues at the EM lab for their help with electron microscopy. Ashley Sachs, an undergraduate researcher, for collaboration on the boundary characterization of the polymer layers, and Dr. Terry Bruce in biology for her hard work in characterization of our samples, which was not an easy task.

I would also like to acknowledge the South Carolina Space Grant Consortium Funding (REAP Grant: “Alteration and Characterization of Fracture Mechanisms Along Metal-Polymer Interfaces” number SC NASA EPSCoR RID 520797). This work was

also supported by Sandia National Laboratories, a multi-program laboratory operated by Sandia Corporation, a Lockheed Martin Company for the United States Department of Energy's National Nuclear Security Administration under contract DE-AC04-94AL850.

TABLE OF CONTENTS

Page

CHAPTER 4.

CHAPTER 5

LIST OF FIGURES

LIST OF TABLES

CHAPTER ONE

INTRODUCTION TO FLEXIBLE ELECTRONIC SYSTEMS

Flexible electronic systems (FESs) consist of conductive materials incorporated onto compliant substrates [1.1]. These devices must maintain current flow while being stretched by up to ten percent strain [1.1]. FES are lightweight compared to traditional systems [1.2] and are capable of conforming to the shapes different structures, unlike rigid systems which often need flat, level surfaces. Flexible electronic systems are currently being studied for replacement of traditional circuitry in various commercial and military aerospace applications [1.3].

1.1. Introduction to Flexible Systems

For many applications, FES are advantageous when compared to traditional systems. The FES can conform to unique topographies [1.3], have increased yield strength [1.4] and undergo fracture at larger tensile strains [1.5]. The deposition of metal films on polymer substrates is a highly researched topic due to reliability issues seen in multilayered devices. Flexible thin film systems may have the ability to sustain larger amounts of strain to failure than their bulk counterparts. However, adhesion of the film on the substrate fails before high strains are reached.

Flexible electronic systems are beneficial because they have the potential to be thin [1.2], have increased corrosion resistance [1.6], have increased barrier properties [1.7], a good heat distortion range [1.7] and are able to be manufactured to cover large areas. This makes them ideal for harsh environments and the moderate temperature fluctuations seen in aerospace applications including: space borne telescopes [1.8],

synthetic aperture radar [1.9], solar sails, active surfaces [1.10], extraterrestrial balloons [1.10] and large antennae structures [1.1]. Metallic films deposited onto polymer substrates exhibit desirable properties including the ability to be conformed to the surface to which they are adhered, the potential for large scale fabrication [1.7] and low production costs [1.12].

1.2. Types of Flexible Electronic Systems

Flexible electronics became popular in the 1980's [1.13] when the semiconductor industry began to thin down silicon wafers to decrease manufacturing costs. By backing electronics systems on to a flexible polymer substrate, they were able to create flexible LCD displays, [1.14] as seen in Figure 1.1. Over the past thirty years, engineers have sought to increase the compliance of the systems by both changing the substrate material and also using "origami" forming. Currently, there are several different substrates used for FES including [1.15], glass [1.7], polyimide [1.16], and stainless steel [1.16]. Engineers also noticed that by designing these normally rigid systems in unique geometries, such as a twist [1.17] or buckle [1.17] the devices will straighten out when strain is applied to them.

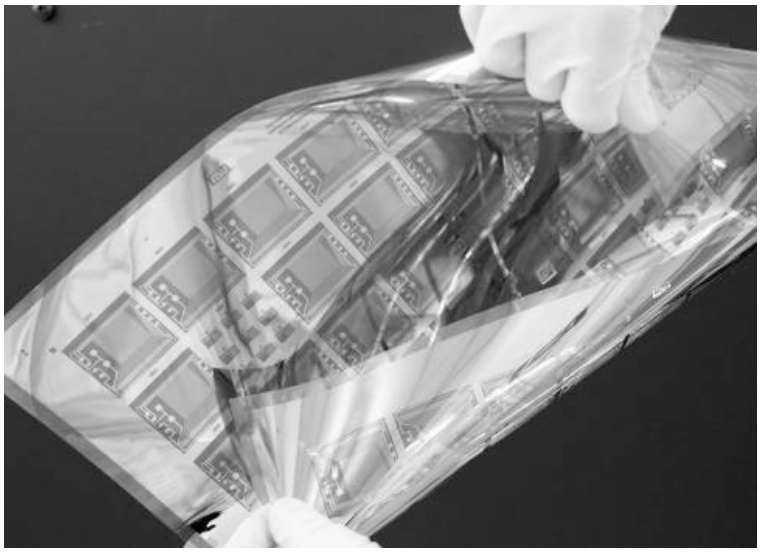

Figure 1.1: Flexible amorphous silicon backplane on Gen II PEN substrate made at Arizona State University [1.16]. This image shows the large amount of bending that flexible systems can under go.

1.3. Roll-to-Roll Processing and Other Common Fabrication Methods

Traditional semiconductor devices are made by lithographic processing, which is a long and expensive process only capable of patterning small areas at a time [1.14]. Photolithography is commonly used in semiconductor industry [1.13]. It is where electronic components are patterned onto silicon substrates, most commonly silicon wafers, through a series of masks, depositions and chemical etching [1.14] that may have to be repeated multiple times depending on the device [1.15]. In this system, the process starts will silicon. FES, on the other hand, start with large rolls of sheet metal, polymer or glass. Flexible systems can be manufactured by a roll-to-roll (R2R) processing [1.2], ink-jet printing [1.6] and photoablation [1.15]. Flexible systems have the potential to be produced in large quantities at low cost [1.1]. R2R processing is a continuous method (Figure 1.2.) where electronics can be patterned on to flexible rolls in a multistep process.

Some general steps are: deposition, patterning and packaging, which can happen a various number of steps depending on the device.

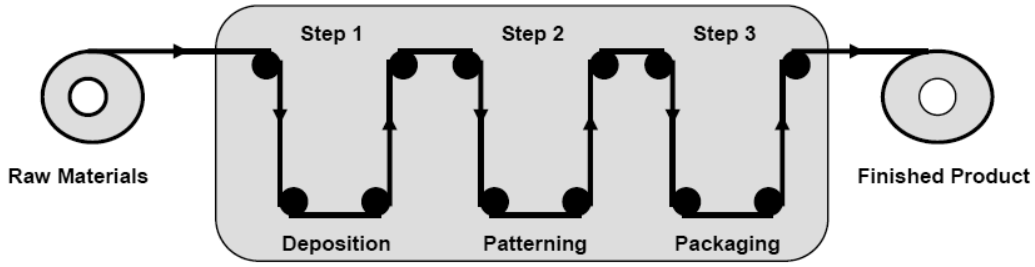

Figure 1.2: Roll-to-Roll processing has three general steps: deposition, patterning and packaging [1.6]. The polymer substrate starts out as a roll, metallic films are deposited (step 1) and then patterned (step 2). In step 3 the electronic system is packaged by encapsulation.

During inkjet printing is like using a printer, only instead of standard ink, metallic lines or conducting "ink" are deposited on to a flexible substrate [1.18]. This process is commonly used to deposit silver lines or joints onto electronic circuitry. Photoablation uses high precision lasers, ultra-violet light and vapor deposition [1.11] to pattern a series of high-resolution lines and devices directly onto flexible substrates. It has higher resolution and is able to pattern continuously, make smaller devices then photolithography [1.15].

1.4. Reliability and Lifetimes of Flexible Electronic Systems

One reliability issue associated with electronic devices is the ability of the metallic lines to conduct and remain adhered to the substrate for the component lifetime [1.19]. Failures, such as buckling [1.20], wrinkling [1.21] and cracking [1.22] can all lead to shorting of the metal lines, or debonding and crossing [1.20], which resulting in a loss of

current flow [1.17]. To improve the lifetime and durability of these devices, the metallic films to stay adhered, or joined to, the flexible substrate must be improved.

1.5. Fractures in Thin Film Systems

Previous work on both traditional electronic systems and model flexible systems has identified some contributing factors to the interface fracture [1.23]. These include the film residual stress [1.1], thermal mismatch between the film and substrate [1.24] and poor adhesion [1.1] which is the ability to remain chemically bonded to the substrate. Residual stress is an internal stress in the material that develops due to processing procedures, thermal cycling or plastic deformation [1.25]. Excessive stresses in a material may lead to cracking [1.13]; buckling, when the film delaminates from the substrate [1.13]; and wrinkling, when the film and substrate deform spontaneously [1.26]. If the residual stress is tensile, it will cause cracking across the surface, which may cause interface delamination or propagate cracks into the surface of the substrate [1.22]. If the residual stress is compressive will result in buckling, which relieves the elastic strain energy or energy needed for deformation or delamination. The residual stresses seen in films often develop due to processing.

Thin films deposited by deposition often develop high residual compressive stresses during the deposition process. The large stresses (1 GPa) developed may cause nucleation and growth of blisters, or circularly debonded areas, over initially debonded surfaces [1.27]. When the strain energy release rate exceeds the film's interfacial toughness delamination occurs between the film and substrate.

Hutchinson and Sou have proposed multiple ways to characterize the strain energy release rate in thin films by including a dimensionless driving force depending on the cracking pattern [1.22] observed in the devices. Hutchinson and Sou assumed elastic bodies under an axial load, with no shear (only a bending moment) at the crack tip [1.28]. If all relevant quantities such as the film modulus, stress and thickness are known, it should be possible to predict crack trajectory. This crack follows the most energetically favorable path and the mode at crack tip will also determine the type of cracking seen in the film.

The stress field at the crack tip governs the mode, or load relative to the crack tip. When in tension, the crack will be in pure mode I and the crack will propagate along the interface, and in mode II, the crack will continue into the substrate [1.22]. Mixed modality at the crack tip means the crack may be driven off the interface into the substrate or along the substrate interface [1.22]. The mode of failure depends on the Young's modulus, Poisson's ratio of the substrate and the film thickness. The effect of film thickness on interfacial toughness is associated with crack nucleation. Films debond when the strain energy within a system is greater than the interfacial adhesion energy [1.29].

When a thin-film buckles, it can form various morphologies, such as a straight edged buckle or a telephone cord buckle, where the crack follows a sinusoidal path [1.27]. Thin films on substrates can also wrinkle, which is when the film deforms the substrate but does not de-adhere from the substrate [1.21]. When taking into account films buckling on compliant substrates, the mode at the buckle wall changes from mode I to increasing

mode II [1.30]. There are numerous studies that characterize delamination on rigid substrates, but there has been little work done on modeling compliant substrates [1.30]. Work done by Cotterell et al. has shown compliance has a large effect on the fracture energy and phase angle of loading. When the substrate is more compliant, the mode I contribution is increased and increases the chance of failure. In order to accurately model thin-film behavior and improve the reliability of flexible electronics, it is important to understand the energy needed for delamination and failure.

1.6. Recent Advancements in Deformation of Metal-Polymer Interfaces

Thin-film systems have properties that are more advantageous than their bulk counterparts including higher hardness, strength and wear resistance [1.31]. Thin-film behavior is often governed by surfaces, interfaces and their adhesion. Metal films on polymer substrates deform by strain delocalization, where the film debonds from the interface and forms a neck. This process allows metal films on polymer substrates to sustain up to 30% elongation before rupture [1.32]. The ability of thin films to debond and elongate without rupture will be discussed further in Chapter 2.

1.7. Mechanically Testing Roll-to-Roll Specimen

Currently, bulge testing is only used on wafers or small batches made in laboratories. Roll-to-roll processing is cheaper and more effective than using photolithography for applications with a large area. Bulge testing would be an ideal way to test large-scale flexible electronics that can be produced during roll-to-roll. The advantage to bulge testing is a novel way to extract materials properties from a composite system without the permanent damage [1.29].

1.8. Research Intent

The intent of this research is to better understand how model flexible thin film systems deform due to both intrinsic and extrinsic stresses. Using model film systems (Au/Polyimide, W/PMMA and W/Polystyrene), the effect of substrate compliancy on film fracture and the unique behavior of these systems will be compared to different rigid systems; this is discussed in Chapter 2. Multiple methods of characterizing thin film systems discussed in Chapter 3. The effect of film thickness, chemistry and stress on adhesion and fracture will be presented in Chapter 4. In Chapter 5, modifications to a bulge test system will be made, in addition to adding a heater to test for the effects of heat on flexible systems. Future work is discussed in Chapter 6.

1.9. References

[1.1] N. Lu, et al., "Metal films on polymer substrates streched beyond 50%," Applied Physics Letters, vol. 91, pp. 1909-1912, 2007.

[1.2] S. Lacour, et al., "Design and Performance of Thin Metal Film Interconnects for Skin-Line Electronic Circiuts," IEEE, vol. 25, pp. 180-183, 2004.

[1.3] W. Xu, et al., "Effects of interfacial properites on the ductility of polymer-supporetd metal films for flexible electronics," International Journal of Mechanical Solids, vol. 47, pp. 1830-1837, 2010.

[1.4] K. T. Jia, E. Ma, "Effects of nanocrystalline and ultrafine grain size on constitutive behavior and shear bands in iron," Acta Materialia, vol. 51, pp. 3495-3509, 2002.

[1.5] D. Silbernagl, et al., "Influence of Film-Substrate Adhesion on the Mechanical Properties of Thin Polymer Films," American Chemical Society, vol. 25, pp. 5091-5097, 2009.

[1.6] A. Gregg, et al., Flexible Flat Panel Displays: Wiley, pp 12-15, 2005.

[1.7] S. Chin, "Roll-to-roll flexible displays still far from reality," EETimes, vol. 2010, pp. 456-478, 2006.

[1.8] T. Nakamura and S. Kamath, "Three-dimensional effects in thin film fracture mechanics," Mechanics of Materials, vol. 13, pp. 67-77, 1992.

[1.9] E. Brandon, et al., "Flexible Electronics for Space Applicatins," Materials Research Society, vol. 814, pp. 219-230, 2004.

[1.10] H. Jiang, et al., "Mechanics of percisley controlled thin film buckling on elastomer substrates," Applied Physics Letters, vol. 90, pp. 119-133, 2007.

[1.13] S. Lacour, et al., "Strechable Interconnects for Elastic Electronics Surfaces," IEEE, vol. 93, pp. 1459-1467, 2005.

[1.14] W. Wong and A. Salleo, "Flexible electronics: materials and applications," Springer Science and Business Media, pp. 1-10, 2009.

[1.15] M. G. K. e. al., "Analog and Digital circuits using organic thin-film transistiors on ploymer substrates," IEEE Electron Device Letters, vol. 21, 2000.

[1.16] K. Jain, et al., "Flexible Electronics and Displays: High-Resolution, Roll-to-Roll, Projection Lithography and Photoablation Processing Technologies for High-Throughput Production," IEEE, vol. 93, pp. 1500-1510, 2005.

[1.17] S. Venugopal, et al., "Flexible Electronics: What can it do? What should it do?," IEEE, pp. 234-246, 2010.

[1.18] M. Huang, et al., "Metal Films Crawling in Interconnect Structures Caused by Cyclic Temperatures," Acta Materialia, vol. 49, pp. 3039-3040, 2001.

[1.19] Sirringhaus, "High Resolution inkjet printing of all-polymer transitor circuits," Science, vol. 290, pp 67-76, 2000.

[1.20] B. Balogh, et al., "Qualification and Reliability Tests of Flexible Printed Circuits," IEEE, vol. 2, pp. 2108-2115, 2007.

[1.21] M. W. Moon, et al., "The charaterization of telephone cord buckling of compressed thin films on substrates," Journal of Mechnical Physical Solids, vol. 50, pp. 2355-2377, 2002.

[1.22] S. Goyal, et al., "Buckling, Wrinkling and Debonding in Thin Film Systems," IEEE, vol. 987, pp. 4C 3.1-10, 2010.

[1.23] J. W. Hutchinson and Z. Sou, "Mixed mode cracking in layered materials," Advances in Applied Mechanics, vol. 29, pp. 63-191, 1992.

[1.24] G. Parry, et al., "Effect of substrate compliane on global unilateral post-buckling of coatings: AFM observations and finite element calculations " Acta Materialia, vol. 53, pp. 441-447, 2005.

[1.25] R. Koch, "The intrinsic stress of polycrystallin and epitaxial thin metal films," Journal of Condensed Phyiscal Matter, vol. 6, pp. 9515, 1994.

[1.26] W. D. C. Jr., Material Science and Engineering an Introduction. Hoboken, NJ: John Wiley & Sons, 2003.

[1.27] H. Mei, et al., "Fracture, Delamination, And Buckling of Elastic Thin Films on Compliant Substrates," IEEE, vol. 9, pp. 1232-1243, 2008.

[1.28] M. J. Cordill, et al., "Adhesion measurements using telephone cord buckles," Material Science and Engineering A, vol. 443, pp. 150-155, 2007.

[1.29] S. Li, et al., "The effects of shear on delmanination in layered materials," Journal of Mechanics and Physical Solids vol. 52, pp. 193-214, 2004.

[1.30] A. A. Volisnky, et al., "Interfacial toughness measurement for thin film substrates," Acta Materialia, vol. 50, pp. 441-466, 2002.

[1.31] B. Cotterell and Z. Chen, "Buckling and cracking of thin films on compliant substrates under compression," International Journal of Fracture, vol. 104, pp. 169-179, 2000.

[1.32] D. L. Smith, Thin-Film Deposition, McGraw-Hill Inc, 1996.

[1.33] Y. Xiang, et al., "High ductility of metal film adherent on a polymer substrate," Applied Physics Letters, pp. 321-330, vol. 87, 2005.

CHAPTER TWO

METALLIC THIN FILMS: DEPOSITION, DEFORMATION AND FRACTURE

The properties of metallic thin films often are different than their bulk counterparts [2.1]. Metallic coatings and thin films are often utilized because of their increased yield strength [2.2], fracture resistance [2.2] and improved electrical conductivity [2.3]. Coatings can range from between a few microns to hundreds of millimeters thick [2.4], and a thin film ranges from a fraction of a nanometer to a few microns thick [2.2].

The physical properties of thin films are unlike than those of bulk material. This size effect seen in thin films gives them superior properties such as: high yield stress due to limited dislocation mobility [2.5], low electrical resistance over many periods of strain cycling [2.6] and the ability to conduct applied electrical current at small thickness [2.7]. These unique properties have led to many applications for metallic thin films such as oxide and corrosion protection [2.2], metallic interconnects for semiconductors [2.8], magnetic layers for memory devices [2.9], Microelectomechanical systems (MEMS) [2.10] and reflective and anti-reflective layers in optical devices [2.11].

This chapter will give an overview of the types of metallic coatings used for electronic systems (Section 2.1) and methods for depositing these metallic thin films (Section 2.2). The type of deposition parameters that control the metallic thin film structure will be explained in Section 2.3. Then methods to characterize film deformation will be discussed in Section 2.4. An overview of recent characterization of flexible systems (Section 2.5) will be given.

2.1. Types of Metallic Thin Films Used for Electronic Systems

Metallic films deposited for electronic systems must have a low resistivity, low defect concentration, high purity and high conductivity to carry an electrical current [2.12]. Typical metals used as conductive lines in electronics systems are gold (Au), Silver (Ag), copper (Cu) and aluminum (Al) [2.13].

Table 2.1: Properties, including conductivity, modulus and hardness, of materials commonly used materials for conductive thin films.

Material	**Electrical Conductivity (s/cm)**	**Modulus (GPa)**	**Hardness (GPa)**
Gold	$2.0*10^5$	78 [2.14]	10 [2.15]
Silver	$2.6*10^4$ [2.16]	67 [2.16]	6 [2.16]
Copper	$7.9*10^4$ [2.17]	83 [2.18]	13 [2.18]
Aluminum	$4.8*10^3$ [2.19]	72 [2.20]	10 [2.19]

2.2. Metallic Thin Film Deposition

There are many methods to deposit metallic thin films, they include: electrochemical deposition, physical vapor deposition (PVD) and chemical vapor deposition (CVD) [2.21]. In electrochemical deposition, an electric field is used to transfer metal ions using a negative charge to attract positive ions to the substrate in an electrolyte solution. Electroplating is a common electrochemical deposition used to put a coating on substrates using Cu, Au or Ag as a plating material. Electroplated films often have high impurity concentrations due to contamination from the electrolyte source. During PVD, in vacuum ions in plasma are accelerated with an electric current or magnetic field towards a pure metal target, bombarding the target atoms, ejecting them and depositing them on a substrate [2.21]. An advantage of physical vapor deposition is it allows for the film properties to be altered by varying the processing parameters [2.2].

In CVD, the film source is a gas that is chemically converted into a vapor and deposited onto the surface of the substrate. CVD is typical used to deposit dielectric films, however it is used to deposit metallic lines when the features size is too small to use PVD or deposition other techniques [2.22]. The purity of CVD and PVD is higher than that of electroplated films [2.15].

2.3. Thin Film Structure

The deposition technique, material of both the film and substrate, and thickness of the film will determine the type of structure that will occur. By controlling the partial pressure and substrate temperature can control the film growth kinetics. These factors will dictate how the film grows and the film's microstructure the film will have.

In order to know where the adatoms will go on the surface it is important to know the energy of the surface configurations. The more bonds that are formed with the surface, the less likely it is an atom will move to another point along the surface [2.37]. Once adatoms begin to for clusters or islands they will also form imperfections such as terrace or ledge structures [2.27]. These features will act as nucleation sites for other adatoms with contribute to film growth [2.37].

A film will grow by the nucleation of islands that occur when adatoms have enough energy to nucleate and grow. As the adatoms begin to grow they will orient themselves in low energy orientations that directly affects the crystal orientations of the film [2.23]. As the number of low energy islands increases atoms begin to diffuse away from less favorable energy islands toward the low energy islands and allows them to coalesce [2.2]. The film will continue to coarsen as islands with low surface and

interfacial energy controlling the crystallographic orientation and grain structure of the film [2.23].

Work done by Thorton characterizes the effects of changing the temperature of the substrate and/or the argon pressure will affect the grain structure. Thorton used a structure-zone diagram to show that thin film microstructure fell into four zones: Zone I. low argon pressure results in tightly packed, fibrous or cone like grains with many voids and defects. Zone T. where there are less defects and voids but the cone like structure of Zone I. Zone II, slightly higher temperatures allow for increased diffusion and produces columnar grains and Zone III which is above temperatures of 0.5 of the melting temperature, equiaxied grains occur due to annealing of the film [2.24]. Thorton demonstrated the importance processing parameters on grain structure as seen in Figure 2.1. Grain structure plays a large role in the stress in a film [2.21]. By altering the processing parameters it is possible to control not only the grain structure by the stress in a film.

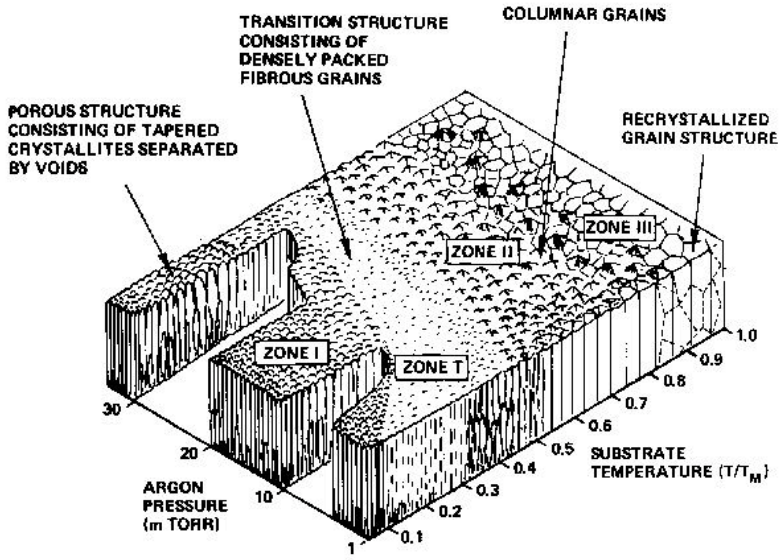

Figure 2.1: The structure and residual stress of metallic thin film are controlled by the processing pressure and substrate temperature during sputter deposition. This figure shows schematically the structure-zone diagram relating pressure and temperature to grain structure [2.24].

2.4. Stress in Thin Films

Stresses are present in all thin films and can affect adhesion, crystalline defects and film topography [2.21]. Thin film behavior can be dictated by residual stress, and thermal expansion [2.25]. If these stresses are relaxed it can lead to de-adhesion or tensile cracking. The stresses seen in thin films are intrinsic, thermal and extrinsic stresses.

2.4.1. Intrinsic Stress

Intrinsic stress, or the internal stress due to structure and properties of the material, may be resultant from processing parameters, as discussed above, because they dictate how a film can grow and develop a highly compressive or tensile stress. By using the processing pressure of argon to control the energy of the ions in gas and the flux of

sputtered atoms different stress can result and change the inherent stress state of the film. Compressive stresses often arise through the development of voids from high-energy bombardment [2.26]. The high-energy bombardment causes the surface atoms to be closer to each other forming a closely packed film at low temperatures. This process is similar to shot-peening, used to put surfaces in compression [2.27]. As pressure continues to increase and the films density increases the voids begin to break and islands begin to coalesce forming low angle grain boundaries and resulting in a tensile stress in the film [2.2]. As these films continue to grow they begin to develop grain boundaries, voids, impurities and domain walls. As grain growth continues recrystallization occurs, and hillocks form at the grain boundaries from diffusion of the film material to the surface along grain boundaries. This increased diffusion makes the grain boundaries high stress areas. This can lead to large stress in the film, which will continue to develop as the temperature is decreased.

2.4.2. Thermal Stresses

Differences in the thermal coefficient of expansion between the film and the substrate can result in residual stress. A film that under goes thermal cycling as a result of application can undergo stress variations. These stresses can also arise if the film is sputtered at an elevated temperature and cooled to room temperature. If the film is attached to the substrate and is not allowed contract the resultant stress is tensile, likewise if a film is not allowed to expand it will result in a compressive stress [2.26].

2.4.3. Epitaxial Stress

An epitaxial stress arises because of crystallographic mismatch between the film and the substrate. If the mismatch between the two is large you will have increased mismatch strain in the film. However if there is good lattice match the film will have relatively low stress due to a low number of grain boundaries [2.28]. As the film grows it begins to orient itself in the most favorable direction for growth, as the thickness increases lattice mismatch is accommodated by the introduction of misfit dislocations [2.2].

2.5. Mechanical Properties of Metallic Films

It has been established that thin films behave differently than their bulk counterparts, for example, exhibit improved mechanical properties such as higher elastic modulus, higher yield stress and improved hardness. Films that are constrained by a substrate by elastic interactions can increase the yield stress [2.5]. Their behavior can also be dictated by residual stress, thermal and elastic mismatch and a larger density of impurities [2.25].

2.6. Reliability of Thin Films

The reliability of these thin film systems is determined by the interface. This means, that over the lifetime of the film where external stresses, strains and temperature variation are applied [2.29] the film must not fracture through the film or delaminate from the surface.

If the compressive stress is greater than the fracture toughness of the interface then the interface can wrinkle or buckle. If the tensile stress is too high the film may peel or crack and propagate throughout the film. Many models have been proposed to calculate

the interfacial toughness of thin films systems and take into account various geometries, materials, driving forces and fracture mechanisms [2.10], but few take into account substrate compliance. When using a compliant system deformation of the substrate needs to be considered and the energy release rate adjusted to show substrate compliance.

When a metallic film is deposited on to flexible polymer substrate, it behaves differently than a free standing metal film, which can only withstand strains of about 1% strain [2.30] before failure. However, when bonded the polymer substrate it prevents strain localization and necking of the film [2.31]. Finite element analysis show that ductile films properly adhered to a polymer substrates should be able to elongate until the substrate fails [2.32]. Although most experiments show elongations of less than 20% [2.31, 2.33, 2.34], recent experiments by Lu et al. have demonstrated that good adhesion between metal polymer films is possible by sustaining elongations of more than 50% [2.35].

Adhesion describes the ability of the film to remain bonded to its substrate and is a property of the material. Poor adhesion can lead to failure for many electronic applications. For good adhesion the chemical bond between the layers must be strong. Chemical bonds only reach tenths of a nanometer so contamination can play a role in de-adhesion. The difference in chemical bonding between materials can play a role in adhesion as well; for example metals bond well with oxides due to the formation of bridging chemical bonds [2.3]. The semiconductor industry uses this technique to bond gold films to silicon wafers using an aluminum oxide interlayer [2.21]. However, if the film and the substrate have significantly different bonding methods it will be harder for

them to bond to each other [2.2], it because of this that the reliability of the metal polymer interface of is of such importance. The two most common failure modes of flexible systems are fracture and interface delaminating.

These studies provide the motivation for enhanced adhesion. If the adhesion of metal polymer thin film systems can be improved, they could endure drastically higher strains this will improve durability and expand the applications of these systems, more on adhesion will be discussed in chapter 4.

2.7. Summary

The processing of thin film systems is a critical step in influencing the residual stress in a film. Depending on these parameters a film may have excessive compressive or tensile stresses. If these stresses are present in flexible electronic systems their reliability may be compromised. Film substrate interfaces may fail because of thermal mismatch, stresses due to processing steps or due to surface flaws. Buckling or wrinkling due to excessive compressive stress may cause shorts in electrical devices. Under tension channel cracking can cause electrical flow of an appliance to stop, resulting in a failure of the device. It is important to understand that these properties are important to controlling the device and preventing failure.

Metallic thin films often have a smaller grain size than bulk materials. They also may have a high degree of texturing from the processing parameters. Due to the size of the grains, these films have a higher density of grain boundaries, which provide easy diffusion pathways for atoms, this can increase electromigration or atomic diffusion

driven by electronic flux [2.36]. Dislocation motion in crystalline thin film materials is constrained by the small grain size and elastic interactions between the film and substrate.

2.8.References

[2.1] E. Pellicer, et al., "Nanocrystallin Electroplated Cu-Ni: Metallic Thin Films with Enhanced Mechanical Properties and Tunable Magnetic Behavior," Advanced Functional Materials, vol. 20, pp. 983-991, 2010.

[2.2] D. L. Smith, Thin-Film Deposition McGraw-Hill Inc, 1996.

[2.3] C. H. F. Peden, et al., "Metal/Metal-Oxide Interfaces: A Surface Science Approach to the Study of Adhesion," Journal of Vacuum Science Tehcnolgy, vol. A9, p. 1518, 1991.

[2.4] P. C. Pinto, et al., "Thin FIlm Coating for Suppressing Electron Multipacting in Particle Accelerators," in Particle Accelerator Conference, pp. 1-9, New York, New York, 2011.

[2.5] W. Nix, "Mechanical Properites of Thin Films," Metallurgical Transactions A, vol. 20, pp. 2217-2245, 1989.

[2.6] S. Lacour, et al., "Design and Performance of Thin Metal Film Interconnects for Skin-Line Electronic Circiuts," IEEE, vol. 25, pp. 180-183, 2004.

[2.7] K. Youssef, et al., "Ultrahigh Strength and high ductility of bulk nanocrystalline cooper," Applied Physics Letters, vol. 87, pp. 91-93, 2005.

[2.8] M. J. Cordill, et al., "Fracture and Delamination of Chromium Thin Films on Polymer Substrates," Metallurgical Transactions A, vol. 41A, pp. 870-874, 2010.

[2.9] S. Frank, et al., "The relationship between thin film fragmentation and buckle formation: Synchrotron-based in situ studies and two-dimensional stress analysis," Acta Materialia, vol. 57, pp. 1442-1453, 2009.

[2.10] A. A. Volisnky, et al., "Interfacial toughness measurement for thin film substrates," Acta Materialia, vol. 50, pp. 441-466, 2002.

[2.11] W. R. Runyan and K. E. Bean, Semiconductor intergrated circuit procesing technology Reading, Massachusetts: Addison-Wesley, pp.10-25, 1990.

[2.12] K. Jain, et al., "Flexible Electronics and Displays: High-Resolution, Roll-to-Roll, Projection Lithography and Photoablation Processing Technologies for High-Throughput Production," IEEE, vol. 93, pp. 1500-1510, 2005.

[2.13] M. Huang, et al., "Metal Films Crawling in Interconnect Structures Caused by Cyclic Temperatures," Acta Materialia, vol. 49, pp. 3039-3040, 2001.

[2.14] K. Gall and J. Diao, "The strenght of gold nanowires," Nano Letters, pp. 561-569, vol. 5, 2004.

[2.15] X. Li, et al., "Direct nanomechanical machining of gold nanowires using a nanoindenter and an atomic fore microscope," Journal of Micromechanics and Microengineering, vol. 15, pp. 551-560, 2005.

[2.16] S. Cuenot, et al., "Surface tension effect on the mechanical properties of nanomaterials measured by atomic force microscopy," Physical Review B, pp. 349-359, vol. 69, 2004.

[2.17] S. Swada, et al., "Micropattering of copper on a poly(ethylene terephthalate) substrate modified with a self-assembled monolayer," American Chemical Society, pp. 67-78, vol. 8, 2006.

[2.18] D. Beegan and S. Choedhury, "Work of indentation methods for determing copper film hardness," Surface and Coatings Technology, vol. 192, pp. 57-63, 2005.

[2.19] T.-Y. Zhang and W.-H. Xu, "Surface effects on nanoindentation," Journal of Material Research vol. 17, pp. 1715-1723, 2002.

[2.20] R. Saha, et al., "Indentation of a soft material on a hard substrate: strain gradient hardening effects," pp. 49-56, vol. 9, 2001.

[2.21] M. Ohring, Reliability and Failure of Electron Materials and Devices: Academic Press, Boston, pp 1-34, 1998.

[2.22] S. Roth, et al., "Properties of Tungsten Thin Films Produced with the RF-Sputtering Techniques," Journal of Low Temperature Physics, vol. 151, pp. 216-222, 2008.

[2.23] C. V. Thompson, "Structure evolution during processing of polycrystalline films " Annual Review Material Science, vol. 30, pp. 159-190, 2000.

[2.24] J. A. Thorton, "Influence of appartus geometry and deposition conditions on the structure and topography of thick sputtered coatings," Journal of Vacuum Science Technolgy , vol. 11, pp. 666-670, 1974.

[2.25] J. W. Hutchinson and Z. Suo, Mixed Mode Cracking in Layered Materials: vol. 29: Academic Press, Inc., New York, pp. 76-115 1992.

[2.26] R. Daniel, et al., "The origin of stress in magnetron-sputtered thin films with zone T structures," Acta Materialia, vol. 58, pp. 2621-2633, 2010.

[2.27] F. M. d'Heurle, "Metallurgical Topics in Silicon Device Interconnects: Thin Film Stresses," International Material Reviews, vol. 34, 1989.

[2.28] R. Koch, "The intrinsic stress of polycrystallin and epitaxial thin metal films," Journal of Physical Condensed Matter, vol. 6, pp. 9515, 1994.

[2.29] E. Brandon, et al., "Flexible Electronics for Space Applications," Materials Research Society, vol. 814, pp. 219-230, 2004.

[2.30] R. R. Keller, et al., "Tensile and fracture behavior of free-standing copper films," Material Science Engineering , vol. A 214, pp. 42-58, 1996.

[2.31] Y. Xiang, et al., "High ductility of metal film adherent on a polymer substrate," Applied Physics Letters, pp. 90-101 vol. 86, 2005.

[2.32] T. Li and Z. Sou, "Ductility of thin metal flims on polymer substrates modulated by interfacial adhesion," International Journal Solids Structures, pp. 34-47, vol. 44, 2006.

[2.33] S. P. Lacour, et al., "Strechable gold conductors on elastomeric substrates," Applied Physics Letters, vol. 82, p. 2404-2411, 2003.

[2.34] M. Hommel and O. Kraft, "Deformation behavior of thin copper films on deformable substrates," Acta Materialia, vol. 50, p. 3935-3945, 2001.

[2.35] N. Lu, et al., "Metal films on polymer substrates strained beyond 50%," Applied Physics Letters , vol. 91, p. 221-234, 2007.

[2.36] W. R. Runyan and K. E. Bean, Semiconductor intergrated circuit processing technology. Massachusettes: Addison-Wesley Reading, pp. 115-120, 1990.

[2.37] Nicholas, J. F, *The terrace-ledge-kink (TLK) model,* Springer Material, vol b604, p. 324, 2007

CHAPTER THREE

METAL-POLYMER CHARATERIZATION TECHNIQUES

Testing the mechanical response of either thin films or thin film systems is a challenge to due their small dimensions. However, sometimes the material properties change from the bulk to thin film form (see Table 3.1), there is a need to test these systems. For this reason new test methods, such as the bulge tester, have been developed to extrapolate the materials properties of thin film systems. This chapter will discuss different postmortem characterization methods to determine fracture properties such as atomic force microscopy, scanning electron microscope and confocal microscopy techniques and describe a way to mechanically characterize metal-polymer film systems (bulge testing).

Table 3.1: The bulk and thin film moduli can be different. It is important to note that the moduli can vary by 28%.

Material	**Bulk Modulus (GPa)**	**Film Modulus (GPa)**	**Films Thickness (nm)**
Iron	211 [3.1]	260 [3.2]	1100 [3.2]
Tungsten	410 [3.1]	411 [3.3]	400 [3.3]
Gold	78 [3.1]	91 [3.3]	150 [3.3]
Aluminum	70 [3.1]	90 [3.4]	300 [3.4]

3.1. Scanning Electron Microscopy For Looking at Metal/Polymer Interfaces

Scanning electron microscopy (SEM) is an imaging technique that uses electrons to examine the surface of a sample. In a SEM, electrons are generated by passing voltage through a tungsten or hexaboride (LaB6) filament. The beam is attracted to the surface by an anode and focused to a fine point by a series of condenser lenses [3.5]. When the

beam strikes the surface it interacts with the atoms and emits a secondary electron or other radiation [3.5]. The beam can be rastered across the surface by a series of electromagnetic coils while a detector senses the radiation emitted from the sample. A cathode ray tube (CRT) detects the contrast of the sample and causes the intensity of the light to change. The surface of the sample is a made of many spots on the CRT, which are amplified and displayed on a computer screen.

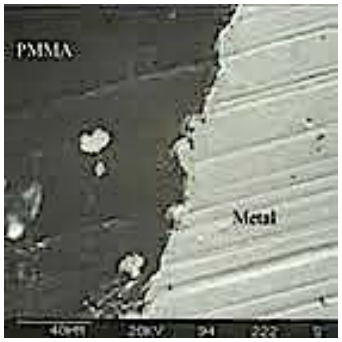

Figure 3.1: A SEM image of a metal deposited onto a PMMA, SEM analysis allows the interfaces of metal-polymer systems to be examined [3.6] in better detail than optical analysis. This image shows the importance of a metal-polymer interface for a hip joint.

A SEM is ideal for studying samples on the nanoscale because of its ease of use and high resolution, high magnification and high depth of field. In an SEM image a large amount of the surface is able to be in focus concurrently, allowing a wide number of features to be studied. It allows for the fracture surfaces and grain morphology to be examined. It is also ideal for metal/polymer interfaces to be examined along with fracture morphologies [3.7]. The high magnification allows for examination of films with small feature size [3.5]. However, SEM has limited magnification, which limits resolution, and don't have the ability to accurately quantify heights of surface features.

3.2. Atomic Force Microscopy

Atomic Force Microscopy (AFM) is used to determine grain size measurements as well as surface roughness of a sample on the atomic level. It is capable of producing quantitative measurements of film topography and relevant microstructural features that can't be determined from SEM analysis. However, unlike the SEM, the AFM can produced artifacts from the tip due to a broken tip or a contaminated tip [3.8]. An AFM uses a fine tip, microfabricated from Si or Si_3N_4, at the end of a cantilever beam. The tip is held at a constant distance from the surface by inter-atomic forces between the atoms of the tip and the atoms composing the sample. The tip across the sample allowing the tip to follow the topography of the sample. As seen in Figure 3.2, a laser is focused on the tip and the deflection of the tip is measured by a photodiode. The force is determined by measuring the vertical deflection of the lever, and measured by a change in voltage.

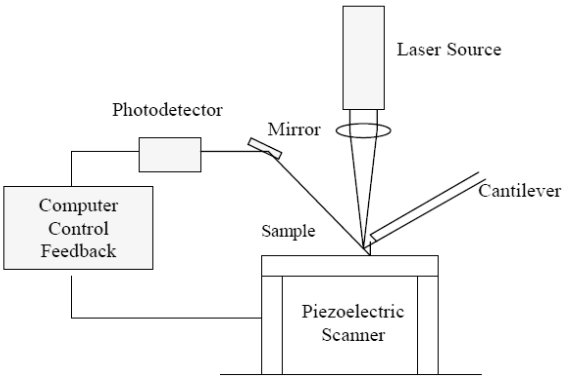

Figure 3.2: (a) A schematic of an atomic force microscopy, an instrument that measures topography of a sample surface [3.9] and a topography image of microcracking seen in a thin copper film on a polycarbonate substrate after tensile testing [3.5].

The AFM has been modified to scan a variety of different surfaces. The two most common modes are contact and tapping. In contact mode, the tip is held at a constant distance above the surface of the sample as it is scanned across the surfaces the tip reacts to changes in the attractive or repulsive forces of the sample the peizo adjusts the tip to maintain a constant distance and a voltage feedback system is used to produce a topography image. Contact mode is useful when examining surface morphology, grain size or roughness, however when used at large loads the tip can indent the surface or ruin surface features.

In tapping mode, the tip oscillates close to its resonate frequency, it is brought towards the surface during scanning until it is lightly tapping the surface. As the tip comes in contact with the surface the frequency changes, the changes in frequency are used to produce measurements of the surface of the samples [3.10]. Tapping mode allows for the measurement of delicate samples and samples with high adhesive or electrostatic forces.

Films deposited with a large compressive stresses form spontaneous buckles, or blisters. These structures are easily observed by AFM. Because of its high spatial resolution AFM is ideal for analyzing the structures of buckling.

3.3. Confocal Microscopy

Confocal microscopy is a light microscopy technique that allows for a large depth of field. This technique is commonly used to observe large-scale changes and shows great promise for quantifying deformation of substrates in the z-direction. By constructing a 3D image of the surface of the sample, confocal microscopy allows you to examine the

surface over a wide rage of focal planes.

Confocal microscopes work by using small apertures are used to make sure only in focus light is capable of being imaged. In confocal imaging, a single point of reflected light is illuminated by an aperture or laser beam in the focal plane of the sample. The light out of focus light is descanned for out of focus light and filtered through a dichoric fliter and focused onto a pinhole. With only this point illuminated, the out of plane light falls off in intensity, thus only focused light in the focal plane of the specimen is allowed through the pin hole. The light that passes through the pinhole is picked up by a photodetector and recorded by a computer. The computer then uses software that assembles the 2D image one pixel at a time. It combines the different focal planes of the sample to create a 3D image or z-stack of the sample.

Confocal imagining is often used to look at phases and structures of polymers or the excitation of dyes in biological samples. In a study done by Sheen, Bao and Cooke, confocal imagery was used to study the surface texture of various foods [3.11]. In order to measure the surface texture of the food they optimized the z-stack for high resolution in the z-direction and transformed them in to topographical images. To measure roughness, they drew line segments randomly across the surface of the sample and measure the average deviation.

3.4. Bulge Test Overview

When bulge testing, a thin-film can be thought of as freestanding diaphragm and modeled as plate. However when it is clamped at the edges it becomes a membrane. The strain distribution of the membrane depends on the geometry of the sample, boundary

conditions and the nature of the loading. It is assumed the bending moments at the clamped edge of the membrane are small and deflection is based solely on deflection at the center of the membrane [3.12]. The stress across the membrane is considered constant and in the elastic regime [3.13].

The bulge test is relatively simple, and it is done by binding a membrane at the edges and applying a uniform pressure to one side of the membrane as shown in Figure 3.3. This technique has been used to determine the mechanical properties and residual stresses of the sample.

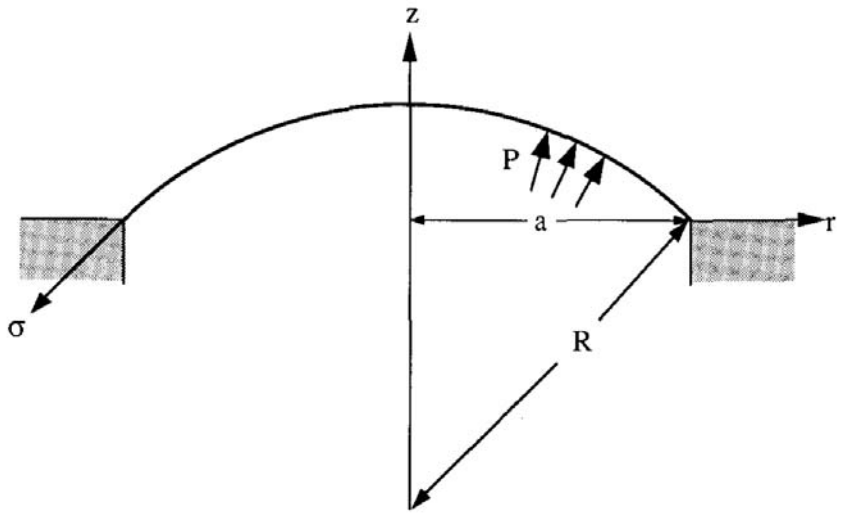

Figure 3.3: This schematic from Small [3.13] shows how a circular clamped membrane deforms as a function of applied pressure (P). The radium of the membrane in this figure is "a" and the radius of deflection is "R".

The stress in the membrane, σ, can be determined by approximating a spherical pressure vessel

$$\sigma = \frac{Pa^2}{4Ht} \tag{3.1}$$

where P is the pressure, a is the half length of the opening, h is the film height and t is the film thickness. Using arc length to find change in elongation, ε, strain in membrane is

$$\varepsilon = \frac{2a}{4h} \tag{3.2}$$

and the constants are the same as in Equation 3.4. Using the stress and strain for an elastic material as they relate to pressure and deflection of the membrane results in

$$P = \frac{8Mt}{3a^2} \tag{3.3}$$

Using just this equation would imply starting out with a virtually flat membrane [3.13] and this scenario is unlikely in most situations. Taking into account residual tension in the film ε_0

$$\varepsilon = \varepsilon_{bulge} + \varepsilon_0 \tag{3.4}$$

$$\varepsilon = \frac{2h}{3a} \tag{3.5}$$

where σ_0 is the residual stress and M is the biaxial modulus.

Using the energy minimization approach used by Vlassak [3.14], which takes into account residual stress and geometry, the relationship between the applied pressure (p) and the height in the center of the membrane (h), is

$$P = C_1 \sigma_0 t \frac{h}{a^2} \tag{3.6}$$

where σ_0 is the residual stress, t is the thickness of the film, C_1 and C_2 are geometrical constants and M is the biaxial elastic modulus. The biaxial modulus is:

$$M = \frac{E}{1-\nu} \tag{3.7}$$

where E is the modulus and υ is the Poisson's ratio which is the same for both bulk and thin film materials. The biaxial modulus can be modified for composite systems to take into account the in-plane deformation of the layers.

$$M_f = \sum_i M_i \frac{t_i}{t_{film}} \tag{3.8}$$

The three most commonly used membrane shapes are a circle, square and rectangle [3.13, 3.14]. Several groups have run finite element analysis on sample geometry to determine C_1 and C_2 as show in Table 3.2 below.

The shape of the membrane being deflected influences the relationship between pressure, deflection and thickness as shown in Equation 3.6. The values for the constants C_1 and C_2 for various sample geometries are listed in this table.

Table 3.2. As the Membrane geometry changes, so do the values for the parameters C_1 and C_2 in equation 3.6. Below are the values for the most common systems.

Membrane Geometry	**C_1**	**C_2**	**Reference**
Spherical Cap	4	2.67	[3.13]
Square	3.4	1.83	[3.14]
Rectangular	2	1.33	[3.15]

It is important to be careful of membrane geometry. A circular opening has equal biaxial stress at the center of the membrane and has no high stress areas, such as seen at the corners in the square or rectangular openings. However, rectangular and square membranes are frequently patterned by etching silicon wafers and are easy to use.

Figure 3.4 shows a pressure deflection curve from a circular membrane of 25 μm Kapton with 100 nm of gold. That uses the model

$$P = Ah + Bh^3 \tag{3.9}$$

to curve fit for the values of A and B which can be used to determine residual stress and biaxial modulus of a composite system.

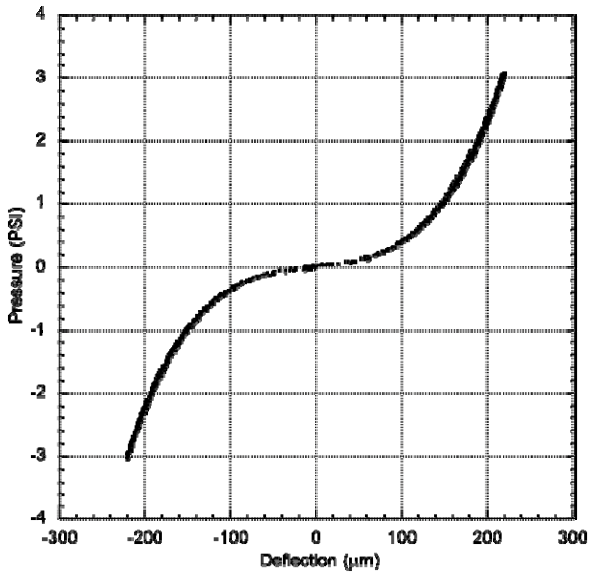

Figure 3.4: This figure shows the predicted pressure-deflection curve for a 6 mm circular membrane. This membrane was assumed to be a uniform composite of 100 nm Au film on 25 μm of polyimide (Kapton). This was made by using equation 3.6 and assuming that the was no residual stress.

The number of studies using bulge testing has increased since due to the perceived decrease in extensive sample preparation for tests including tearing, handling, gripping associated with other mechanical tests. Bulge testing also has the ability to impose loading conditions [3.12].

3.4.1 Clemson University System Design

The Clemson system was designed to be able to both apply a steady pressurization rate and accurately measure the height of the center and also pull vacuum whilst being able to measure the deflection of the membrane. A variation in pressure causes the sample to change position (height). The measurement beam from the laser

interferometer is set to a zero point in the Z-axis. The backscattered light interferes with the reference beam in the scanning head and a photo detector records the interference patterns as a voltage. The voltage is proportional to the velocity of the change in position parallel to the measurement beam. That voltage is then digitized and processed as a vibrometer signal. The signal then converted into a displacement measurement.

The system combines a Polytec MSA 400 laser vibrometer, with a Texas Instruments DP515 Pressure Controller that is recorded and controlled by a PCI6251 USB data acquisition card (DAQ) and NI Labview software. A General Purpose Interface Bus (GPIB) was created to control the amount of pressure and the pressurization rate of the nitrogen gas and a mechanical pump is attached to the pressure controller and is used when negative pressure values are imputed into the VI. The sample holder is in next to a Druck PMP 4060 pressure transducer and an emergence release valve, which sits on top of a microstage that allows for the laser to be centered on the sample.

To run a test, a sample is super glued to the bottom piece of a clamp and allowed to set. The top part of the clamp is then attached using screws and then screwed onto the proper part of the apparatus. The laser is aligned in the center of the sample using the microstage and the focus of the laser vibrometer is achieved using the fine focus knob on the virbometer head. A bar is displayed on the vibrometer head showing the signal strength, when the bar is completely full ideal laser strength has been achieved.

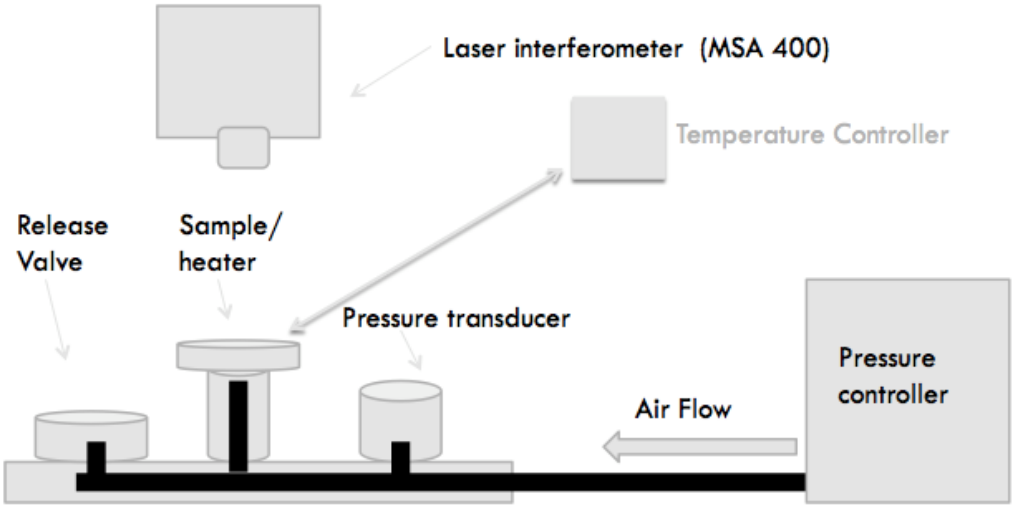

Figure 3.5: Clemson University bulge testing, system pressure flows from the pressure controller to the sample making it deflect and amount of deflection is measured by the laser interferometer. It is capable of controlling temperature of sample.

Once proper alignment is achieved the user can open the virtual interface (VI). The VI interfaces allows for different test parameter settings including precision, and pressurization rate. The pressure is applied and the set point of pressure or vacuum is entered and changed during testing. The parameters used in this study were four decimal places precision and units of pressure per square inch (PSI). Then depending on the test the pressurization rate and maximum pressure were set accordingly. After the proper values are set the run button is pushed and the test can begin, during the set point much be changed manually to cycle from positive to negative pressure. The time in 0.01 seconds, pressure in PSI and deflection in μm are exported as a text file.

The Clemson University bulge test system is unique in that it is one of few systems that have been modified to be able to heat the sample. The system uses two ceramic heating elements are inserted in holes drilled perpendicular to the clamp to heat the

sample. The heaters are regulated by an Omega DNi8 temperature controller using a proportional integral derivative (PDI) loop to maintain a set temperature. The controller uses a J type thermocouple to measure the temperature of the sample. To use the heaters a value is entered as a set point and then an upper and lower value are set in the PDI loop menu.

3.5. References

[3.1] J. William Callister, Material Science and Engineering An Introductioin. Hooboken, NJ: John Wiley & Son's, pp. 879-889, 2003.

[3.2] Z. F.-X. Wen Yu-Hua, Liu Yue-Wu, "The Influence of Grain Size and Temperature on the Mechanical Deformation of Nanocrystalline Materials: Moleculare Dynamics Simulation," Chinese Physics, vol. 10, pp. 407-414, 2001.

[3.3] A. J. Kalkman, et al., "Young's modulus measurements and grain boundary sliding in free-standing thin metal films," Applied Physics Letters, vol. 78, pp. 2674-2677, 2001.

[3.4] J. Menik, et al., "Determination of elastic modulus of thin layers using nanoindentation," Journal of Material Research, vol. 12, pp. 2475-2485.

[3.5] W. R. Runyan and K. E. Bean, Semiconductor intergrated circuit procesing technology Reading, Massachusetts: Addison-Wesley, pp. 567-576,1990.

[3.6] D. S. Gianola and C. Eberl, "The Micro- and Nanoscale Tensile Testing of Materials," Journal of Materials, vol. 61, pp. 24-35, 2009.

[3.7] P. Lin, "The in-situ measurements of mechanical properties of mulitlayer coatings," Ph.D, Massacusetts Institute of Technology, pp. 89-101, 1990.

[3.8] G. Parry, et al., "Effect of substrate compliance on global unilateral post-buckling of coatings: AFM observations and finite element calculations," Acta Materialia, vol. 53, pp. 441-447, 2005.

[3.9] T. Camersano and B. Logan, "Probing Bacterial Electrosteric Interactions Using Atomic Force Microscopy," Enviornmental Science Technology vol. 34, pp. 3354-3362, 2000.

[3.10] S. Cuenot, et al., "Surface tension effect on the mechanical properties of nanomaterials measured by atomic force microscopy," Physical Review B, vol. 69, pp. 34-54, 2004.

[3.11] S. Sheen, et al., "Food Surface Texture Measurement Using Reflective Confoval Laser Scanning Microscope," Journal of Food Science vol. 73, pp. 227-234, 2008.

[3.12] B. E. Alaca and K. B. Toga, "Strain-Controlled Bulge Test," Journal Materiatl Research, vol. 23, pp. 3295-3302, 2008.

[3.13] M. Small and W. D. Nix, "Anaylsis of the accuracy of the bulge test in determining the mechanical properties of thin films," Journal Material Research, vol. 7, pp. 1553-1563, 1992.

[3.14] J. J. Vlassak, "Thesis," PhD, Standford University, pp. 1-67 1994.

[3.15] T. Tsakalakos, "The Bulge Test: A Comparison Of Theory And Experiment For Isotropic And Anisotropic Films," Thin Solid Films, vol. 75, pp. 293-305, 1981.

CHAPTER FOUR

THE ROLE OF FILM THICKNESS, INTERLAYER AND SUBSTRATE THICKNESS IN W/PMMA AND W/PS SYSTEMS

4.1. Introduction to Substrate Compliance and Fracture in Thin Film Systems

In recent years there has been an increased interest in flexible thin films systems and the effect of substrate compliance on fracture. For rigid film/substrate systems it has been shown that as film thickness increases so does the energy need for fracture [4.1]. In rigid systems, fracture is limited to the interface [4.2]. Finite element simulations show that when a film buckles it can plastically deform a compliant substrate, and thus the true work of adhesion is underestimated by not taking into account inelastic deformation [4.3]. A popular model developed by Hutinchson and Sou [4.4] assumed an infinitely thick substrate, which doesn't take into account the stiffness of the substrate relative to the film. To accurately adjust the strain energy release rate to take into account the inelastic deformation of the substrate and the stiffness of the film evidence substrate compliancy need to be taken into consideration.

To demonstrate the effect of substrate compliance of flexible thin film systems, highly stressed tungsten was deposited on polymer systems of polystyrene (PS) and polymethylmethacryalte (PMMA) and the resulting fracture morphologies were studied. An interlayer of aluminum oxide was added to try and improve adhesion and change the chemistry at the substrate interface. The effects of film thickness and interface chemistry on the strain energy release rate were examined and proof of substrate damage will be presented.

4.2. Thin Film Systems used to Examine Substrate Compliance

The samples used for this study were 1 cm by 1 cm by 1 mm polystyrene (PS) and polymethylmethacryalte (PMMA) from Goodfellow Corporation with radio frequency (RF) sputter deposited tungsten (W). The tungsten was deposited with varying argon pressure from 0.4 Pa to 2.0 Pa to impose high compressive stress (HCS) and high tensile stress (HTS) respectively. By changing the argon pressure the intrinsic stress state of the film was changed. When the argon pressure is low there is a resultant higher kinetic energy in the gas, which results in a more densely packed film and becomes compressive. Likewise, if pressure were higher there is a decrease in the kinetic energy of the vapor particle and can result in tensile stress.

Film thicknesses of 200, 400 and 600 nm were deposited onto both the PS and PMMA and were measured using a DETAK profilometer. Then, to change surface adhesion, a set of identical samples were run with a 10 nm aluminum oxide interlayer between the tungsten film and the substrate. The stress in the films were found to be -1.7 GPa for the compressive samples and -1.0 GPa for the tensile samples.

A second set of samples were made by changing the substrate thickness, this was done by spin coating PS onto a copper film (Cu) in varying thicknesses of 13, 100, 300 nm. Then using the same process described above compressive films of tungsten without an interlayer were deposited onto the PS. All samples in this section were prepared at Sandia National Laboratories by N. R. Moody and D. P. Adams.

Table 4.1: Material, thickness and stress of the samples used in this study to test adhesion.

Tungsten on PS/PMMA	Tungsten on PMMA/PS with 10 nm interlayer	Tungsten on PS on Cu
HCS: 200, 400, 600 nm	HCS: 200, 400, 600 nm	HCS W 300 nm on 300 nm PS
HTS: 200, 400, 600 nm	HTS: 200, 400, 600 nm	HCS W 100 nm on 100 n PS
		HCS W 100 nm on 13 nm PS

The films were then examined using an optical microscope, films that were that didn't completely debond or spall were characterized further using an AFM to measure the buckle size and amount of substrate deformation. A SEM was used to find the crack width in the tensile samples.

4.3. Adhesion Measurements in Tensile Films

4.3.1. Work of Adhesion

The true work of adhesion is defined as the energy needed to form a new surface between two materials that are chemically bonded [4.4]. The work of adhesion, W_A is:

$$W_A=\gamma_f+\gamma_s+\gamma_{fs} \tag{4.1}$$

where γ_f and γ_s are the surface energies of the film and substrate and γ_{fs} is the energy of the interface. In Griffith fracture, it is assumed that the $W_A=\Gamma_I$, where Γ_I is interfacial fracture toughness in mode I loading [4.5]. However, in practice it is generally accepted that there is plastic deformation at the crack tip and it is in a mixed mode [4.4]. In this case we are actually measuring the practical work of adhesion W_p:

$$W_p = W_A + \Gamma_{\text{inelastic}} \tag{4.2}$$

where $\Gamma_{inelastic}$ is the amount of energy put in to plastic deformation. In this assumption a various amount of energy is lost to plastic deformation depending on modality of the crack, stress in the film and elastic mismatch between the film and substrate. In order to get close as possible to the true work of adhesion it is necessary to normalize the phase angle.

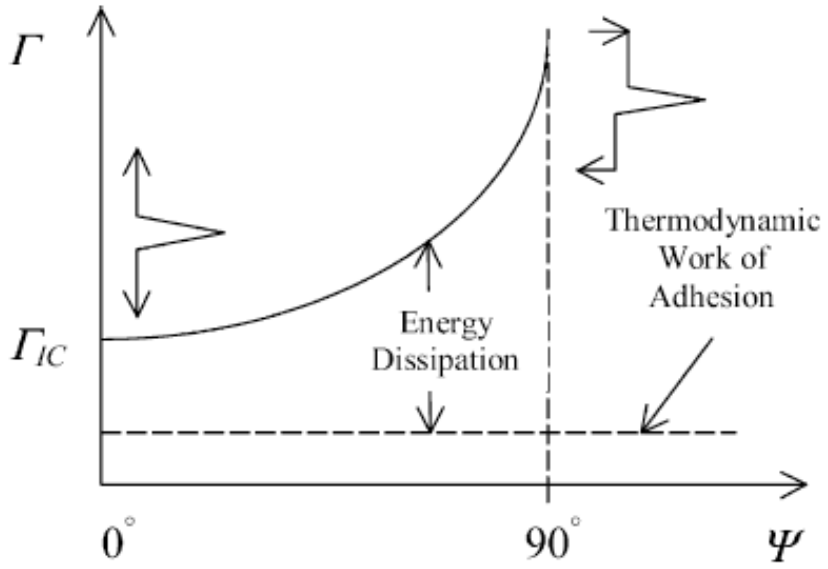

Figure 4.1: Fracture toughness as function of the mode of the crack tip; the closer to mode I the crack tip is the closer it is to the true work of adhesion [4.5].

4.3.2. Fracture Toughness

Abundantly stressed films store large amounts energy per unit area, for example some tungsten films can have up to 1-2 GPa of compressive stress [4.6]. Failure of the interface will occur when the strain energy release rate G exceeds the interfacial fracture energy Γ_i and will continue to propagate until the strain energy is reduced. The energy require to overcome the fracture resistance is:

$$G = Z\frac{\sigma_r h}{E} \tag{4.3}$$

Where Z is a dimensionless driving force that is dependent on cracking pattern and elastic mismatch, σ_r is the residual stress, h is the film thickness and E the biaxial modulus. Assume both materials are isotropic and linearly elastic, any differences in elastic mismatch between the materials can be characterized by the Dundurs parameters α and β. Hutchinson and Sou identified 5 different types of cracking patterns were identified and the dimensionless driving force were calculated under the assumptions of elastic homogeneity and the substrate was indefinitely thick.

The relevant types of cracking for this study are channeling cracks, substrate damage and debonding and will be briefly discussed here. When Z=1.967; channeling cracks occurs which is where cracks propagate through the film until impeded by another crack or the edge of the film, this process will continue until all the stored strain energy is release. Depending on the film's elastic modulus and the Poisson's ration of both the substrate and the film cracks may not arrest at the surface but continue into the substrate and damage it. This cracking is known as substrate damage, where Z=3.951. The last type of cracking seen was debonding of the film from the substrate, the debond may result from other cracks or from defects of the surface of the film; Z=1.028 for the initiation of debonding.

Wrinkling patterns are usually seen in thin film systems with a rigid film on a soft substrate [4.7]. When the film is in a compressive state and is sufficiently attached to the substrate, coherent deformation of both the film and the substrate without delamination is

wrinkling. When the compressive stresses in the film exceeds the critical wrinkling stress, the film will spontaneously wrinkle forming waves in an attempt to lower the elastic energy [4.8]. The critical wrinkling stress is σ_w and E_f and E_s are the elastic modulus of the film and substrate.

$$\sigma_w = \frac{\overline{E_f}}{4}\left(\frac{3\overline{E_s}}{\overline{E_f}}\right)^{\frac{2}{3}} \tag{4.4}$$

The stiffer the substrate the higher the stress needed for cohesive deformation, however if parts of the film delaminate from the substrate and continue along the interface delamination and buckling is said to occur [4.9]. As the film delaminates from the substrate it can grow as a straight-sided buckle or transition into a telephone cord buckle. It has been determined that it is energetically favorable for the crack tip to propagate in such a way that a sinusoidal telephone cord like structure is developed [4.10]. It is not uncommon for a straight sided buckle to develop into a telephone cord buckle [4.11]. The energy required for interfacial fracture is determined by the critical buckling stress σ_b, and the residual stress σ_r.

$$\sigma_b = \frac{\mu^2 E}{12(1-\nu^2)}\left(\frac{h}{b}\right)^2 \tag{4.5}$$

$$\sigma_r = \sigma_b \, C \, \frac{\delta}{h} \tag{4.6}$$

where μ^2 and c_1 are constants that depend on the buckle shape, for a straight-side buckle they are π^2 and ¾ respectively. The stresses are dependent on the h thickness of the film, b half of the buckle width, δ the buckle height and the materials ν Poisson's ration and E elastic modulus.

The interfacial fracture energy, Γ(Ψ), is calculated by the phase angle of the loading as the ratio of shear to normal forces. For a straight-sided buckle it is:

$$\Gamma(\Psi) = \frac{(1-\nu^2)}{2E} \tag{4.7}$$

4.3.3. Problems with Current Models

Much work has been done to characterize buckling of thin films on rigid substrates, however little work has been done to investigate this phenomenon on compliant substrates. Finite element simulations done by Parry et. al. show that some of the elastic strain energy goes into deforming the substrate, meaning that the critical buckling stress $\sigma_{b,}$, has been underestimated [4.12] due to an inaccurate account of the mixed modality at the buckle wall with compliant substrates [4.13].

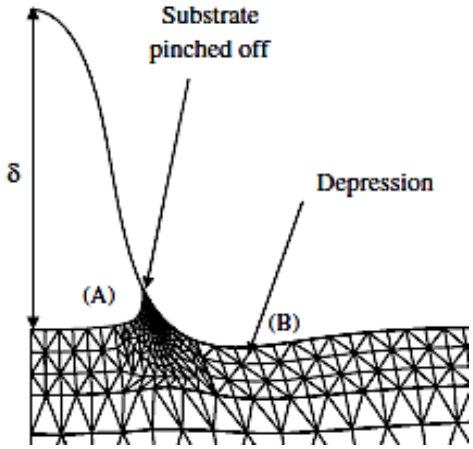

Figure 4.2: Finite element model by Parry et al showing substrate pinching and a deformation zone extending into a polymer substrate [4.12].

The effects of substrate mismatch can be taken into account by considering the Dundurs' coefficient α [4.12, 4.13].

$$\alpha = \frac{\bar{E}_f - \bar{E}_s}{\bar{E}_f + \bar{E}_s} \tag{4.8}$$

The other Dundurs' coefficient β is disregarded as it has little effect on the energy release rate in many models [4.4]. For a very soft substrate α=0.98 and for a rigid substrate α=-1.

4.4. Adhesion Measurements in Tensile Films

4.4.1. Optical Analysis of Tensile Films

The optical analysis of the tensile films revealed extensive debonding of the film from the substrate on the PMMA samples with and without the interlayer. The deadhesion of the film from the substrate was too great for the adhesion energy to be accurately

calculate for those samples. Analysis of the PS samples, displayed in Figure 4.3, showed an increase in crack density with increasing thickness. The introduction of the aluminum oxide interlayer increased the crack density.

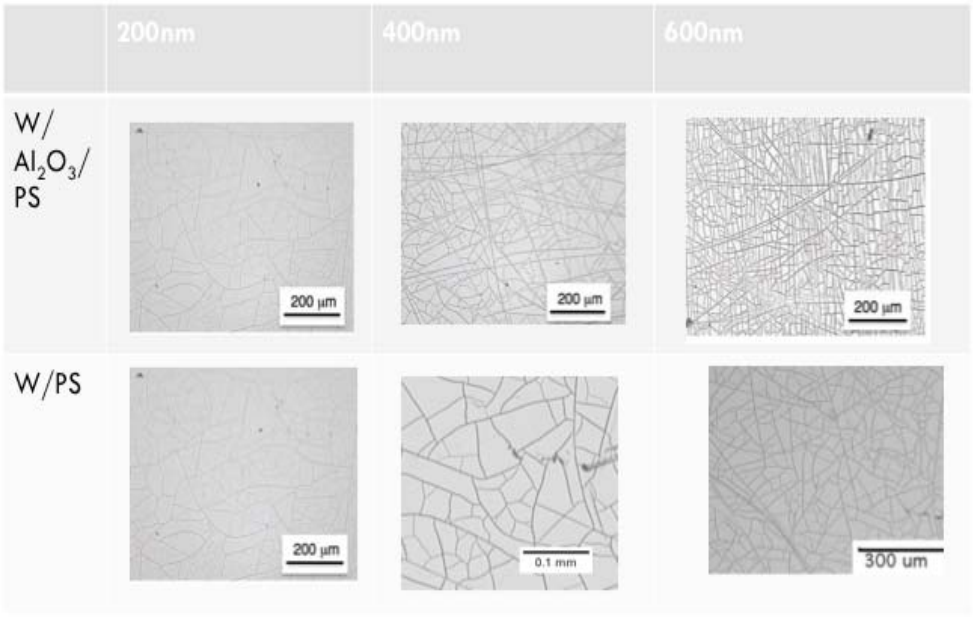

4.3. Optical images of the tensile W/PS systems with and without and interlayer with increasing film thickness. As film thickness increases so does crack density.

4.4.2. Scanning Electron Microscopy Analysis

Crack widths were examined in Hitachi 4800 FESEM, the images were exported into Image J. Crack density was calculated using the Heyn intercept method. Representative photos of the crack width are shown in Figure 4.4.

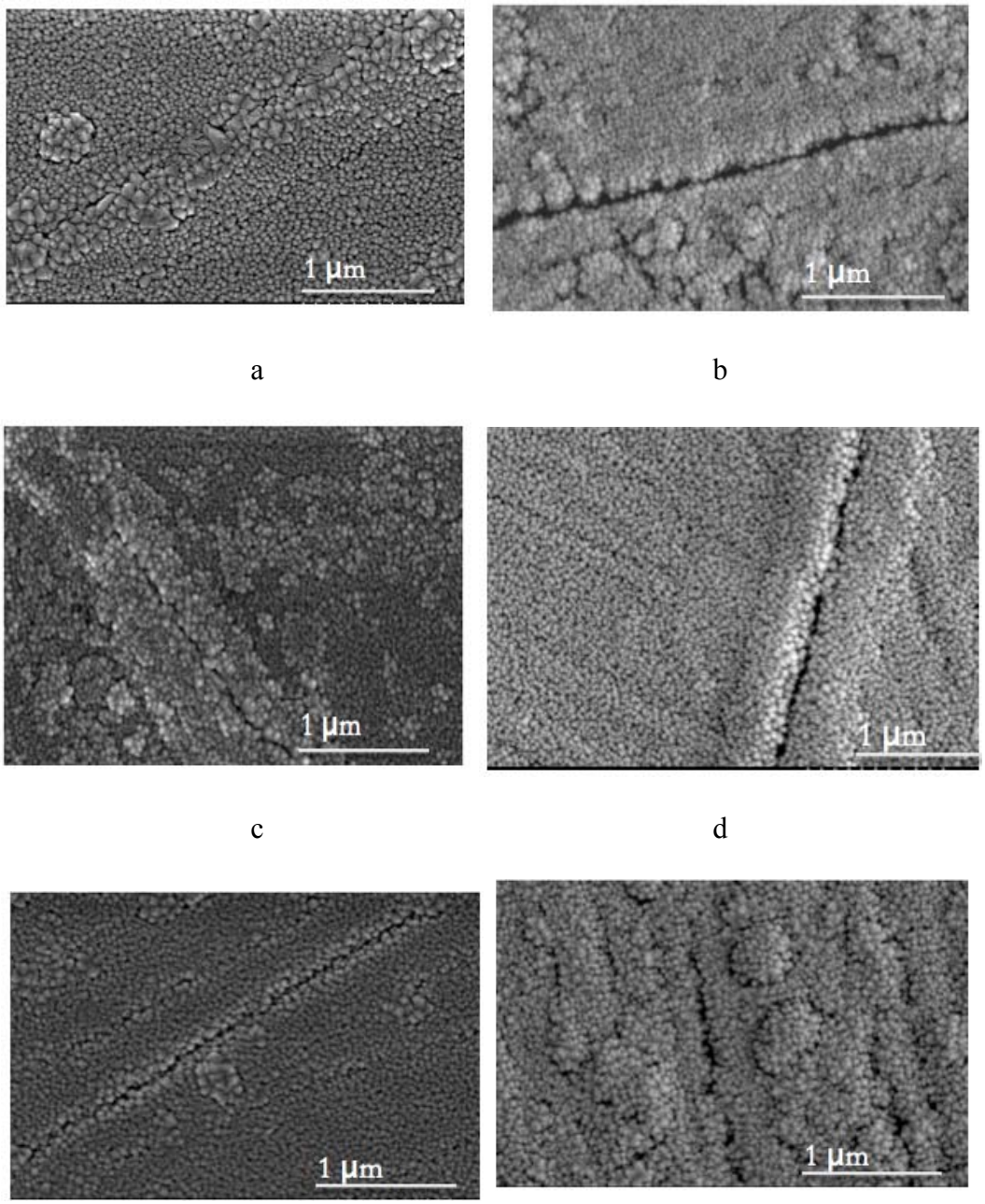

Figure 4.4: SEM of tensile cracking in (a) 200 nm W, (b) 200 nm W 10 nm Al_20_3 (c) 400 nm W, (d) 400 nm W 10 nm Al_20_3 (e) 600 nm W and (f) 600 nm W 10 nm Al_20_3

The crack size increased with increasing film thickness and as mentioned about the crack density increased with increasing film thickness. The samples with the Al_2O_3 had slightly larger crack sizes for all thickness and the crack density increased with the addition of the interlayer.

4.4.3. Adhesion Energy Results for Tensile Cracking

From the images above the crack density and width were used to calculate average strain in the films and then using Hook's law the average stress was found in each sample. Using the average stress the energy release rate was calculated using Equation 4.3. The Z values of Z=1.967 that corresponds to channeling cracks where cracks propagate through the film until it impeded by another crack or the edge of the film was used as an upper boundary. For the lower boundary Z=1.028 for the debonding of the film from the substrate, the debond may result from other cracks or from defects of the surface of the film.

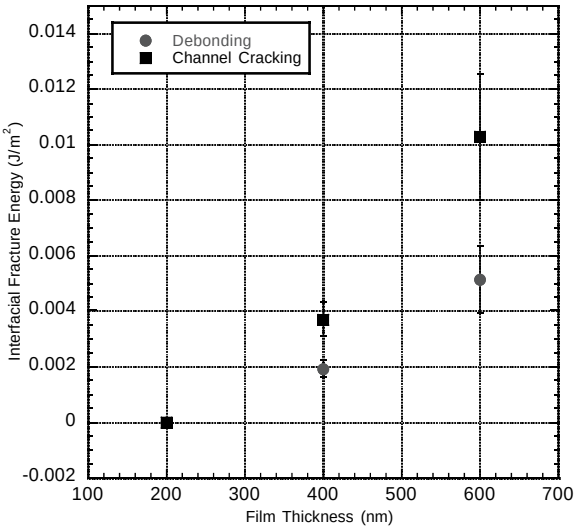

Figure 4.5: Energy release rate of W films on PS without an interlayer for tensile films bound by channel cracking and interface debonding. As film thickness increases so does the engery release rate.

Figure 4.5 shows the values of the strain energy release rate for the 200, 400, 600 nm tungsten films on PS. As the film thickness increase so does the energy release. The values for debonding and channel crack are different indicating that it takes more energy to crack through the substrate than for the film to debond from the substrate. The films with an aluminum oxide demonstrate a similar trend interlayer, as show in Figure 4.6.

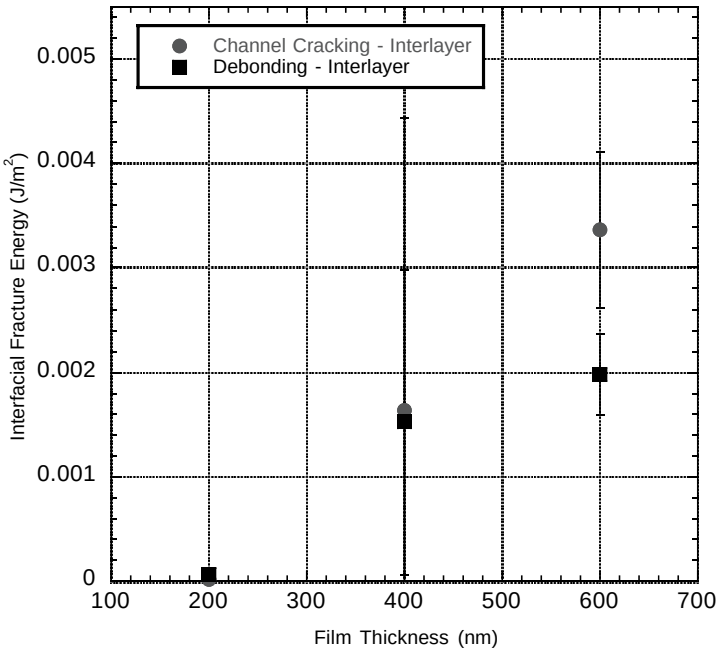

Figure 4.6: Energy release rates for W on PS films with an Al_2O_3 interlayer bound by channel cracking and interface debonding. As the film thickness increases so does the energy release rate.

The aluminum oxide did not improve adhesion. The strain energy release rates were lower for the samples with the interlayer. There isn't much difference between channel cracking and debonding for the 200 and 400 nm films, however for the 600 nm film it takes more energy to have channel cracking throughout the substrate.

4.4. Adhesion Measurements of Compressive Films

4.4.1. Optical Analysis of Compressive Films

An optical analysis of the compressive films revealed that the compressive W films on the PS had completely delaminated and measurements of these films were not possible. The PMMA samples showed straight sided and telephone cord buckles in all

samples. In the 400, 600 nm samples both with and without an interlayer two different buckle morphologies were found; large buckles and small buckles. These two buckles can be clearly observed in Figure 4.7.

4.7. Optical images of compressive W/PMMA systems with and without an interlayer. As film thickness increases different buckle morphology is present.

4.4.2. Adhesion Measurements for Compressive Films

The buckle measurements were taken on a Triboscope AFM in contact mode. The buckle profile was used to get the buckle width w, and height δ. Then using Equations 2.5-7 the interfacial fracture toughness was calculated. As seen in Figure 4.8 and 4.9, the interfacial fracture toughness increases with increasing film thickness for the compressive samples with and without an interlayer. As mention above two different buckle sizes were seen, a larger width buck and a smaller width buckle for film thicknesses of 400 and 600 nm. The fracture toughness was calculated for both sizes of buckles and reported below. The interfacial fracture toughness was approximately the same between the small and large buckles indicating that it takes approximately the same amount of energy to delaminate both

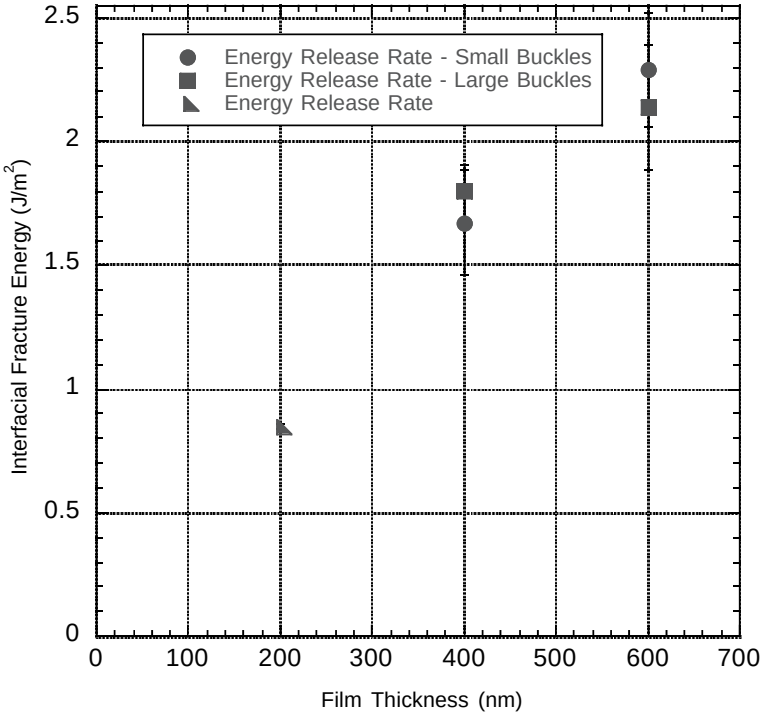

Figure 4.8: Interfacial fracture toughness for compressive tungsten films on PMMA without an interlayer. There is a liner trend, as the film thickness increase so does the interfacial fracture toughness.

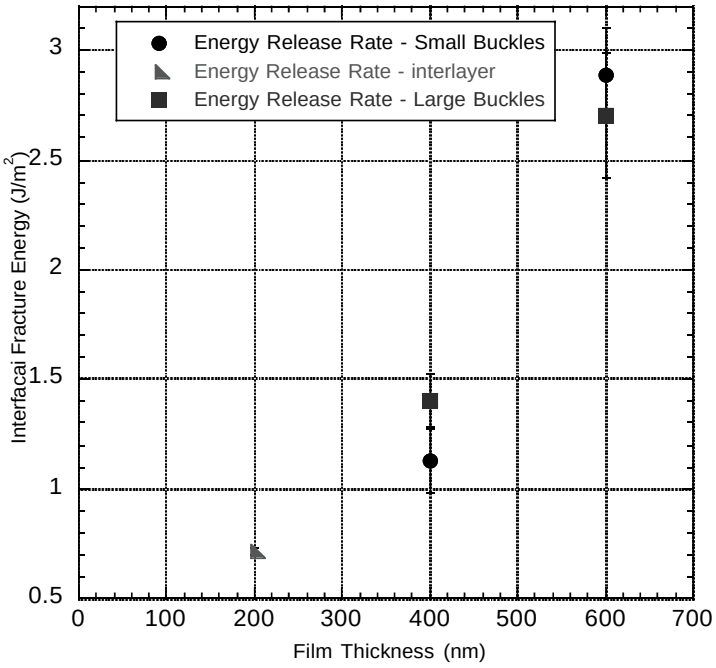

Figure 4.9: Interfacial fracture toughness for compressive tungsten films with an Al_2O_3 interlayer. As film thickness increases so does the interfacial fracture toughness.

4.4.3. Film Thickness Effects on Fracture Energy

As film thickness increased for both tensile and compressive films so did the interfacial fracture energy. As the film thickness increased on the compressive films different buckle morphologies were observed, large and small buckles as seen in Figure 4.8. The adhesion of the films remained the same so the difference in energy can be accounted for by deformation at the film interface. This trend is seen in films deposited onto rigid interfaces also [4.10].

4.4.4. The Effects of Substrate Stiffness and Rigid Interlayer on Fracture

Table 4.2. Values of stiffness, modulus and hardness of the different substrates and the interlayer used to see the effects of stiffness on fracture.

Material	Stiffness (N/mm)	Elastic Modulus (GPa)	Hardness (HRD)	Poisson's Ration
PMMA	84	3	95	0.35
PS	15	3	75	0.35
Al_2O_3	1500	499	1678	0.23

As mentioned above when the tensile PMMA films fractured they pulled away from the substrate in both the films with and without the interlayer. The compressive PS with and without an interlayer peeled up from the substrate. The rigid interlayer promoted cracking in the tensile W/PS films and did not improve adhesion in the compressive films. However, in the compressive films the interlayer did promote the buckle morphology seen in the films without the interlayer, large and small buckle morphology. This demonstrates the importance of taking into consideration the substrate stiffness on interfacial fracture energy calculations.

4.5. Analysis of River Marking Pattern

To confirm deformation in the substrate, the film was removed from the compressive samples and the substrate surface was examined for a river mark pattern left from the film. The pattern was observed optically but due to the transparency of the sample it was hard to as seen in Figure 4.10. For further analysis the river mark patterns were studied using AFM and verified using confocal microscopy. In addition to the 200,

400, and 600 nm HCS tungsten on PMMS, the 13, 100 and 300 nm samples were examined also.

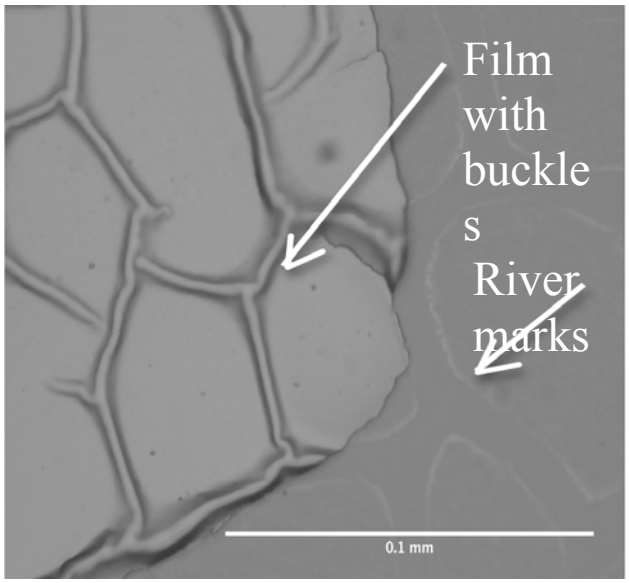

Figure 4.10: Optical image of 300 nm PMMA verifying river marks can be seen and that substrate damaged does occur in compliant substrates.

Using the data from a confocal microscopy the profile was analyzed using Nikon image analysis software a 3-D image was reconstructed of the 13, 100, and 300 nm compressive tungsten on PMMA. Rivermarks were observed in the 100 nm and 300 nm but not the 13 nm sample. For the samples with rivermarks the ratio of the width of the buckle, b, and the height of the deformation zones, d, were measure as shown in Figures 4.12-14.

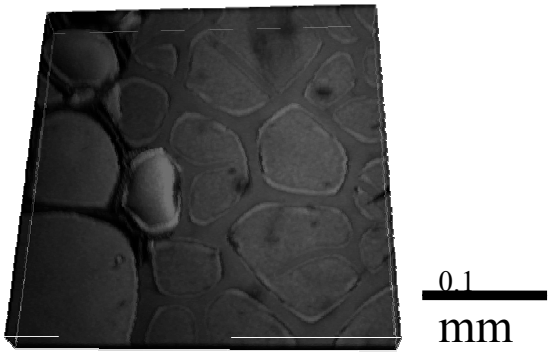

Figure 4.11: A confocal image of 300 nm tungsten on 300 nm PMMA, showing a better view of the substrate damage in compliant substrates.

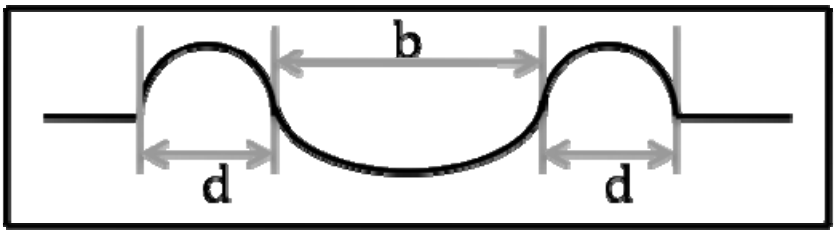

Figure 4.12: A figure demonstrating the how the river marks were calculated, b is the buckle width and d is the width of the deformation zones left by crack tip.

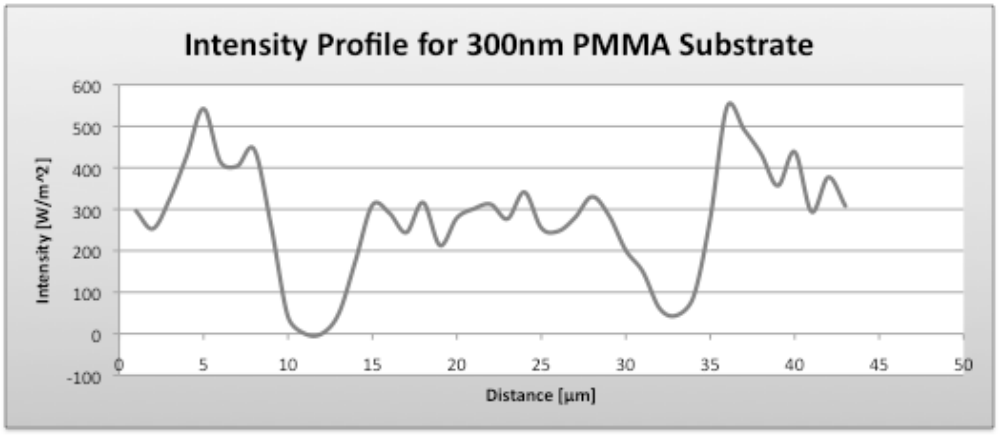

Figure 4.13: An intensity profile from a confocal image of the deformation zones caused by the delamination of a 300 nm W film on 300 nm PMMA.

To confirm the accuracy of the confocal d and b values the samples were also measure in the AFM. Using contact mode the samples were scanned and the rivermarks were verified. Using the surface profile the d and b values were measured using the technique seen in figure 4.15-16.

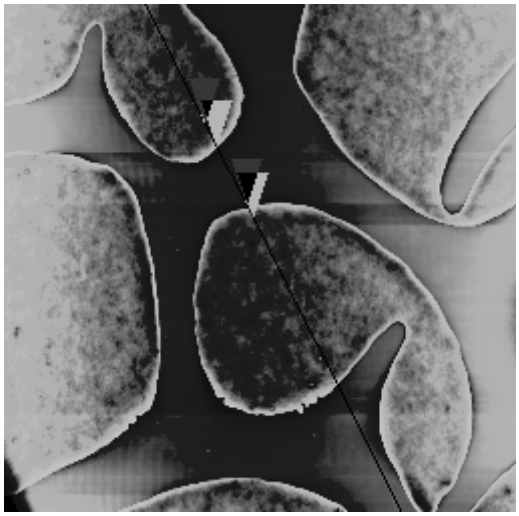

Figure 4.14: AFM image of river marks left in a substrate from a 300 nm tungsten on 300 nm PMMA

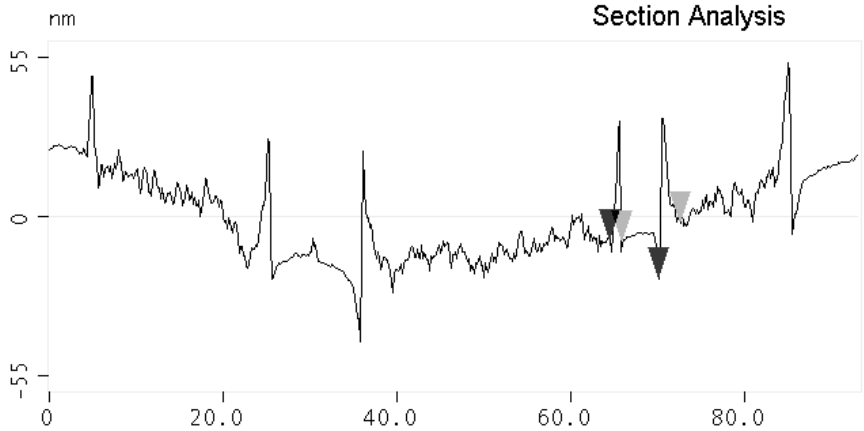

Figure 4.15: AFM surface profile of 300 nm tungsten on 300 nm PMMA demonstrating the buckle width and deformation zone width.

A comparison of the d:b ratios of the confocal and AFM were very close and are shown in Table 4.2 below. For the rest of the compressive the AFM was used to characterize the deformation zones in the rest of the compressive samples.

Table 4.3: The average d:b ratios for two metal-polymer films systems AFM and confocal microscope of river marks on the compressive samples.

Average d:b	**100nm W/100nm PMMA/Cu**	**300nm W/300nm PMMA/Cu**
AFM	0.343	0.232
Confocal	0.285	0.256

The d:b ratios show no overall trend between film thickness, substrate thickness and interlayer. However, in the 400 nm and 600 nm samples with large buckles and small buckles the larger buckles had smaller d:b ratios than the small buckles. The d:b are presented in the Figures 4.17 and 18.

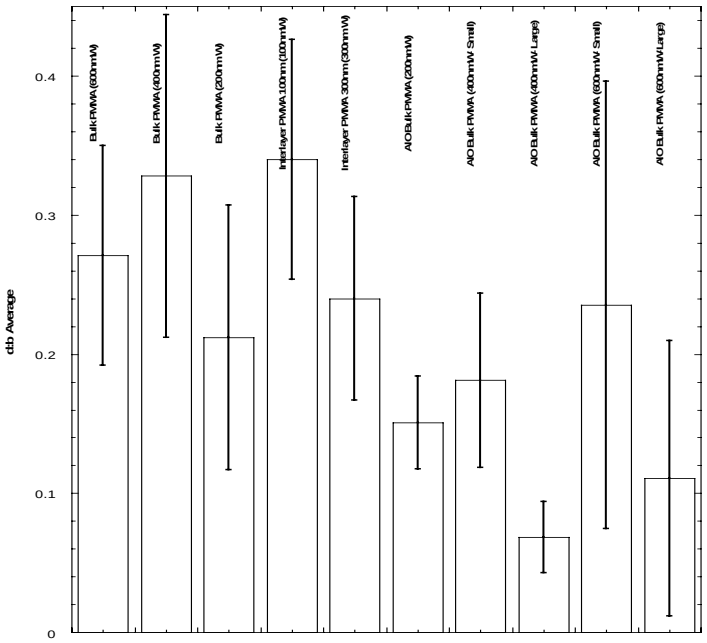

Figure 4.16: The d:b ratios for the compressive tungsten on PMMA with shows no trend for film thickness and substrate damage.

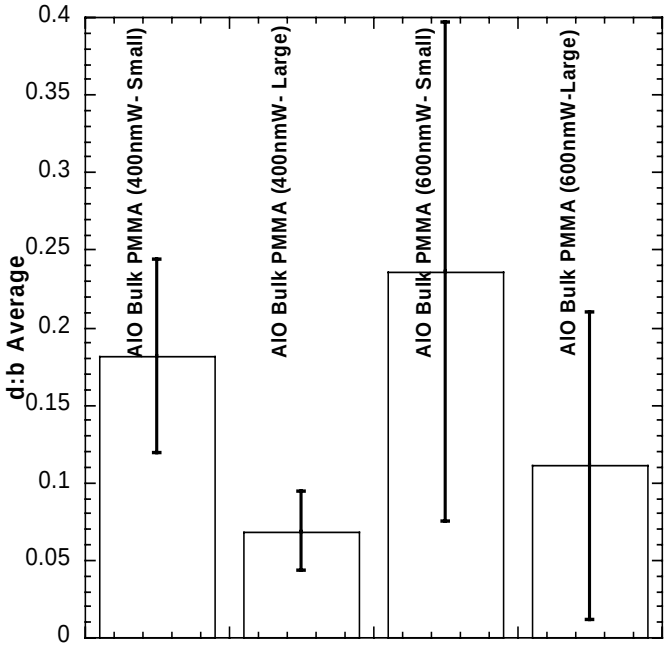

Figure 4.17: Trends can be seen in the samples with large buckles and small buckles in 400 and 600 nm films; as buckle size increases substrate damage increases.

4.6. Discussion and Conclusions

Channel cracking seen in tensile thin films decreases with an increase in film thickness. When cracking occurs in a system with rigid substrate the crack will deflect and continue across the interface. In a complaint system this will be accompanied by debonding from the substrate. Since it is hard to quantify the amount of debonding that will be seen, the values were calculated for pure channel crack for debonding. The actual value will be a combination between channel cracking and interface debonding.

In this study, the interlayer both altered the chemistry of the interface from PMMA/PS with or without an Al_2O_3 interlayer. This created a change in chemistry along with a stiffness gradient. Al_2O_3 has a modulus of 499 GPa compared to 410 GPa and 3 GPa for tungsten and PMMA.

For the compressive films substrate damage is clearly seen in tungsten films on the PMMA substrates. This suggesting that energy goes both into crack propagation along the interface as well as plastic deformation. For metallic films on ceramic substrates, some groups have noted the both the film plastically deforms [4.11] and for films on copper substrates, the substrate deforms [4.14]. The depressions seen by Parry [4.3] and Cordill [4.14] can also clearly be seen in our film systems also. This depression extends past the buckle width to for a depression in the substrate. This take be accounted for by increases the mode mixity at the buckle edge and increased traction in the film [4.1]. On a rigid substrate the buckle edge is assumed to be in pure mode I and there is no deformation in the substrate.

Sample compliance has a significant effect on the energy release rate of thin films on compliant substrates. For thin tungsten films deposited onto PMMA and PS substrates the energy release rate can vary up to 40% [4.12]. In tensile films when channel cracking occurs it often has a component of interfacial debond that isn't seen in rigid substrates. In compressive films buckling included both the film and the substrate. The samples show that deformation of the substrate occurs by leaving river-mark patterns across the sample. This buckling is function wrinkling and buckling and due to the compliance of the substrate the mode mixity at the buckle wall changes. In order to improve adhesion and better understand the fracture of rigid films on compliant substrate and model must be created that takes into consideration the elastic mismatch between the film and substrate.

4.7. References

[4.1] N. R. Moody, et al., "Film thickness effects on the fracture of tantalum nitride on aluminium nitride thin film systems," Engineering Fracture Mechanics, vol. 61, pp. 107-118, 1998.

[4.2] X. Wang, et al., "Effects of substrate orientation and metal film thickness on the intrinsic strenght, intrinsic fracture energy, and total fracture energy of tantalum-sapphire interfaces " Journal of the American Ceramic Society, vol. 88, pp. 1909-1913, 2005.

[4.3] G. Parry, et al., "Effect of substrate compliance on global unilateral post-buckling of coatings: AFM observations and finite element calculations," Acta Materialia, vol. 53, pp. 441-447, 2005.

[4.4] J. W. Hutchinson and Z. Sou, "Mixed mode cracking in layered materials," Advances in applied mechanics, vol. 29, pp. 63-191, 1992.

[4.5] A. A. Volisnky, et al., "Interfacial toughness measurement for thin film substrates," Acta Materialia, vol. 50, pp. 441-466, 2002.

[4.6] P. Waters and A. A. Volinsky, "Stress and Moisture Effects on Thin Film Buckling Delamination," Experimental Mechanics, vol. 47, pp. 163-170, 2007.

[4.7] R. Huang and S. H. Im, "Dynamics of wrinkle growth and coarsening in stressed thin flms," Physical Review E, vol. 74, p. 26214, 2006.

[4.8] R. Huang, "Kinetic wrinkling of an elasric film on a viscoelastic substrate," Journal of Mechancial Physical Solids, vol. 53, pp. 63-89, 2005.

[4.9] S. H. Im and R. Huang, "Wrinkle patterns of anisotropic crystal films on viscoelastic substrates," Journal of Mechanical Physical Solids, vol. 56, pp. 3315-3330, 2008.

[4.10] M. W. Moon, et al., "The charaterization of telephone cord buckling of compressed thin films on substrates," Journal of Mechnical Physical Solids, vol. 50, pp. 2355-2377, 2002.

[4.11] M. J. Cordill, et al., "Adhesion measurements using telephone cord buckles," Material Science and Engineering A, vol. 443, pp. 150-155, 2007.

[4.12] G. Parry, et al., "Effect of substrate compliane on global unilateral post-buckling of coatings: AFM observations and finite element calculations " Acta Materialia, vol. 53, pp. 441-447, 2005.

[4.13] B. Cotterell and Z. Chen, "Buckling and cracking of thin films on compliant substrates under compression," International Journal of Fracture, vol. 104, pp. 169-179, 2000.

[4.14] M. Cordill, et al., "The effects of plasticity on adhesion of hard films on ductile interlayers," Acta Materialia, vol. 53, pp. 2555-2562, 2004.

CHAPTER FIVE

DEVELOPMENT AND CHARACTERIZATION OF A BULGE TESTING SYSTEM FOR ELUCIADATION OF POLYMER MEMBRANE PROPERTIES WITH AND WITHOUT HEAT

Testing thin film mechanical properties and the deformation of membranes can be challenging because of the small feature dimensions, and complex mechanical response. Typically methods used include micro-tensile testing [5.1], nanoindentation [5.2], but thin films are hard to handle and clamp during tensile testing [5.2]. As discussed in Chapter 3, bulge testing allows for the extraction of the composite modulus and residual stress [5.1] of thin films systems. In addition it can be used to test yielding [5.3] of a membrane and the adhesion [5.4] between the film and substrate.

There are many different bulge test designs in literature [5.5]. Table 5.1 summarizes some of the groups in literature that have developed homemade systems. Currently, there are not commercially available systems. This table also summarizes the acctuation and sensing components of these systems. [5.1]. However, there are no significant writings on clamp designs. As shown in Table 5.1 most groups measure the center of deflection of their membranes using a laser interferometer and apply pneumatic pressure. However some groups like Vlassak used a fluid to deflect the membrane. Both of these methods satisfy the model conditions of having uniform loading across the membrane.

Table 5.1: Major groups and institutions that have developed bulge testing systems.

Principal Investagtor	**Institution**	**Measurement Method and Pressurization Method**
J. Kysar	Columbia University	Laser Interferometer/ Pneumatic[[5.6]
J. Vlassak	Harvard	Laser Interferometer/ Hydraulic [5.7]
W. Sharpe	John Hopkins University	White Light Interferometer/ Hydraulic [5.8]
M. Mehregany	Case Western Reserve	Laser Interferometer/ Pneumatic [5.9]
C. Schuh	MIT	Laser Interferometer/ Pneumatic [5.1]
D. Bahr	Washington State University	Laser Interferometer/ Pneumatic [5.10]
T. Tsakalakos	Rutgers University	Laser Interferometer/ Pneumatic [5.11]
C. Lilley	University of Illinois	Laser Interferometer/ Pneumatic [5.12]
R. Vinci	Lehigh University	White Light Interferometer/ Pneumatic [5.7]
M. Kennedy	Clemson University	Laser Interferometer/ Pneumatic

A few groups have started to use bulge testing to look at the response of polymeric membranes and films. They have explored the strain response and effects of film thickness on pressure-deflection curves. Haung et al. found that adding thin polymer films to a SiN_x membrane increased the stiffness of the SiN_x/polymer system [5.13]. This was not predicted by Equation 3.7, where the stiffness of the membrane is proportional to the weighted average of the layer thickness. Another group studied the creep recovery response of polyimide membrane by holding it at constant load. Plotting the

displacement versus pressure they found the polyimide had two distinct regions of deformation: an elastic region and a viscoelastic region [5.14]. This behavior is common behavior for polymers under constant strain below their T_g [5.14], but little has been done to look at how this behavior would change above T_g. A predicted response would be a change in the load-deflection as the glass transition temperature is approached and the polymer becomes more viscoelastic.

5.1. Bulge Testing Chapter Outline

The focus of this chapter is to adjust a bulge test system for both micromachined membranes as well as sheets of film systems produced by roll-to-roll testing. First, to do this, a laser interferometer must be adjusted to the larger deflections seen in flexib5le systems. In order to examine the behavior of a thin polymer film at elevated temperatures, two ceramic heaters were added. A bulge test system that operates above room temperature must be constructed and verified for accuracy. By incorporating a laser interferometer available through the NSF MRI grant the system was optimized to work at room temperature and calibrated to the response of flexible membranes (Section 5.2).

Next, the clamping system was developed for roll-to-roll samples to account for slipping. Then, to simulate possible environmental conditions a heater was added. This allowed us to examine the difference in behavior membranes with polymeric substrates or films at elevated temperatures (23-200°C). By adding a heater, we predict the bulge test system will be able to measure creep [5.3], as well as, strain rate sensitivity [5.16] as function of temperature (Section 5.4).

5.2. Design and Verification of Clemson University Bulge Test System for Room Temperature Testing

In order to repeat tests run by other groups and check the validity of the Clemson University bulge test system, different parameters of the system were optimized and configured to provide reliable results for flexible membranes. Figure 5.1 shows a what a pressure deflection curve of 100 nm of Au on 25 μm Kapton should like.

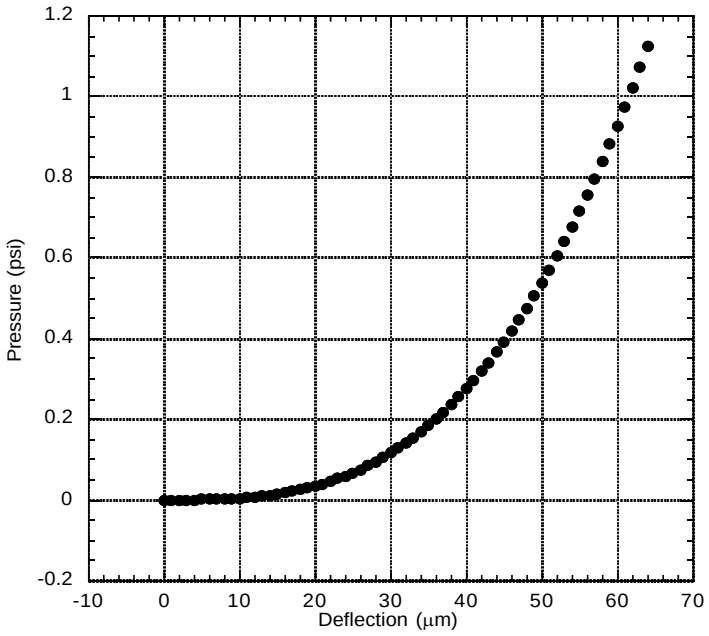

Figure 5.1. What a pressure deflection curve for Au/Kapton with no residual stress should look like. At 0 pressure the membrane is flat, as pressure is applied the membrane deflects.

5.2.2. Fabrication and Characterization of Samples for Bulge Testing

Multiple different sample sets were used to help improve the reliability of the bulge test system. All samples need a reflected coating, all of the membranes were coated with 100 nm of gold (Au). 25 microns (μm) HV Kapton was purchased from DuPont™, and a second system of 100 nm of Au on 200 μm silicon (Si) wafer (Wafer World Inc). The substrates were rinsed with ethanol and then films of 100 nm of gold

was sputter deposited onto the Katpon and silicon wafers in a Kurt J Lesker Co. by RF sputtering using a base pressure (vacuum) was $6*10^{-6}$ torr and the processing pressure was $5*10^{-3}$ (Ar) torr. The power used was 80 watts resulting in a deposition rate of 5.56 nm per second. The height was verified by profilometry.

To use as a comparison, the predicted values for all systems can be calculated and compared to the data from the system. Using Equation 3.8, the theoretical composite biaxial modulus of the system was calculated and these values were used in Equation 3.6. and are presented in Table 5.2. It was assumed due to its thickness and rigidity that the silicon wafer did not deflect. The gold on Kapton system was choose because it's a flexible system with much literature on it.

Table 5.2: Young's Modulus' of the different materials used for bulge testing.

Material	**Young's Modulus**
Silicon Wafer	300 GPa [5.14]
Kapton DuPont™	2.5 GPa [5.13]
100 nm Gold	69.1 GPa [5.15]

5.2.3. Laser Interferometer Settings

The laser vibrometer was designed to measure the deflection of moving systems. Although this system has to measure systems held and a constant pressure with small deflections of over time. So, to test for interferometer stability the laser drift was monitored. To improve the range of measured deflections, 5x objective lens was chosen. To better quantify the laser's ability to measure the deflection of fixed systems over time, a gold (100 nm) coated silicon wafer placed in the clamp and displacement was measured

for an hour. The deflection versus time was plotted in Figure 5.1. Ideally, there should be no change in deflection over time. This figure shows that the laser is jumping.

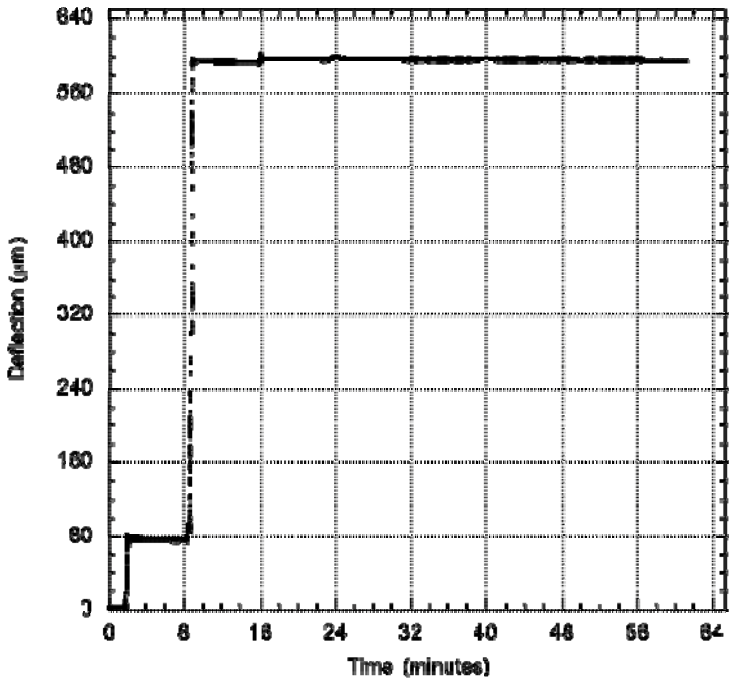

Figure 5.2: Laser drift in a hour of 100 nm on a Si wafer, the laser is meant to measure changes in velocity as a result large jumps in deflection can be seen.

As mentioned the MSA 400 system was designed to measure vibration motion or velocity, so to better adjust the laser to our bulge test set-up settings were adjusted the to fit the properties of flexible systems.

Table 5.3: Adjusted Laser interferometer settings to improve measurements of flexible systems

Parameter	**Old Setting**	**New Setting**
Filters	Low Pass	None
Frequency	5KHz	20 Hz
Window	Hanning	Rectangle
Velocity	125 mm/s/V	1000mm/s/V
Displacement	200 μm/V	50 μm/V
Tracking Filter	Fast	Slow
Low Pass Filter	5KHz	1.5 MHz
High Pass Filter	Off	Off

The new settings gave the laser better resolution and the filters were adjusted to focus on excitations in the lower frequencies and which correspond to more to deflection measurements.

5.3.4. Discussion on Laser Interferometer Settings

By finding the proper setting for the laser interferometer we can ensure that the laser won't lose focus or misread the sample during testing. Metal/polymer systems are less rigid than metal or ceramic systems, by changing the sensitivity and the range of focus we are able to account for the larger deflection seen in these systems. The jumps seen are the laser interferometer resetting the voltage to zero not the membrane actually deflecting. As seen in Figure 5.2 after adjusting the settings and changing the lens the bulge tester was able to make 10 runs of positive and negative pressure with the curves

laying on top of each other. Verifying the system can take measurements at room temperature.

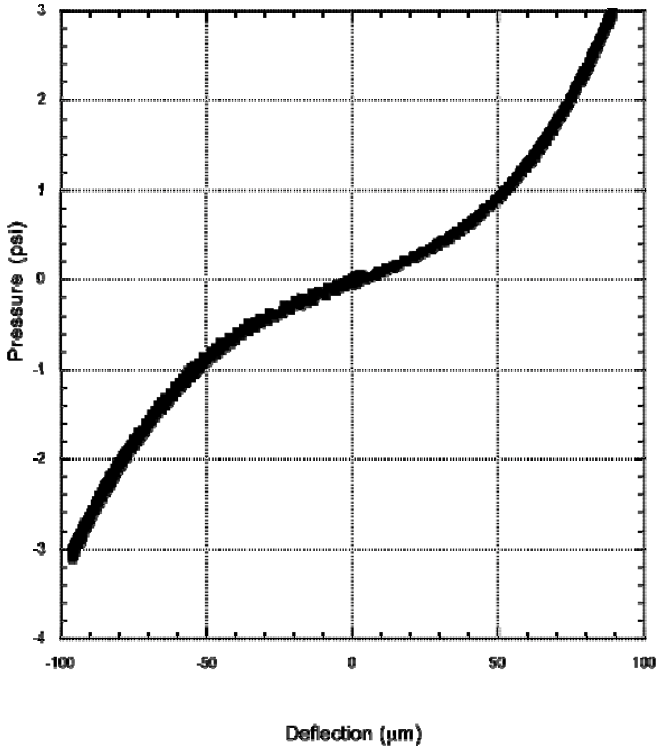

Figure 5.3. 10 runs of the Au/Kapton system of positive to negative pressure. The curves lie on top of each other demonstrating the bulge tester can take reproducible measurements at room temperature.

5.4. Improving the Accuracy of the Clemson University Bulge Test System

Most bulge testers are used to study micro-machined membranes [5.10]. In this section, changes will be made so the system can be used for flexible thin film membranes.

5.4.1. Improving Clamp Design

The bulge test system was first designed using two washers and a sleeve to hold the sample. Using a strain rate of 0.1 psi/s a sample of 100 nm of Au on 25 μm of Kapton was used. The sample was pressurize to 3 psiI/s and then cycled to -3 psi/s and repeated 10 times. Initial data from the bulge test showed a large amount of variability between cycles (load-displacement cycles) in addition to slipping, or where the sample would "pop" while transitioning from positive to negative pressure. During the slipping the laser vibrometer would lose focus and the deflection when transition between pressure and vacuum would be miscalculated as shown in Figure 5.2.

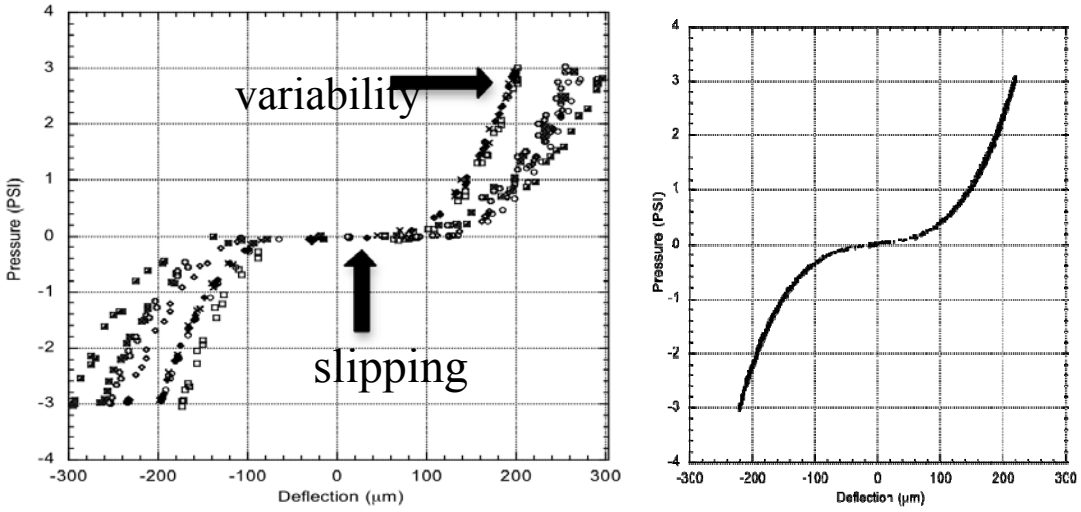

a b

Figure 5.4: (a) Bulge test data showing large variability in the pressure-deflection curves of the 100 nm Au/25 μm Kapton. These in the clamp with the sleeve with arrows pointing to the slipping and variability. Ideally, 10 cycles would all lay on top of each other, like in (b).

In order to decrease the of the large variability and slipping seen in the Au/Kapton system a variety of different clamps were designed. Figure 5.5 shows the original set-up of the bulge tester. Through trial-and-error various materials, lengths of pressure values and clamping mechanisms were tried. The original bulge tester used a four-inch pressure valve and sleeve to clamp the sample between two washers.

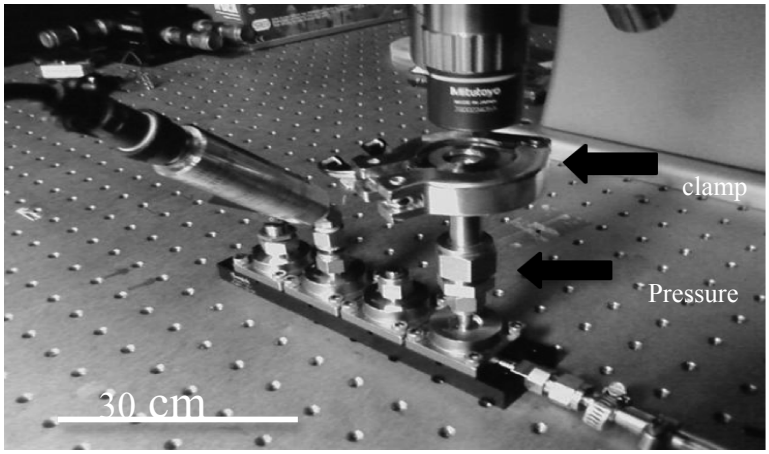

Figure 5.5: Original bulge test set up used a sleeve to clamp the sample between two plates (as shown in the image) This set-up allowed a slow leak and was evident at low strain rate tests.

To improve on the original clamp, a Radel clamp was built that connected to the pressure valve with a flathead machine screw and nut, next a 6160 aluminum (Al) clamp was made that screw into the value and used screws to secure the sample. Finally, an Al clamp that held the sample with screws and was machined to screwing to the bottom half of the pressure valve was made and yield the most consistent results. Figure 5.5 shows the various clamp designs. All clamps had a 6 mm circular hole for the sample. The final design improved the overall variability but there was slipping of the sample. To fix this issue super glue (cyanoacrylate) was used around the hole of the clamp to secure the film

in place and prevent the film from slipping the clamp. After this point all samples were tested in a Al clamp with 6 mm diameter circular opening.

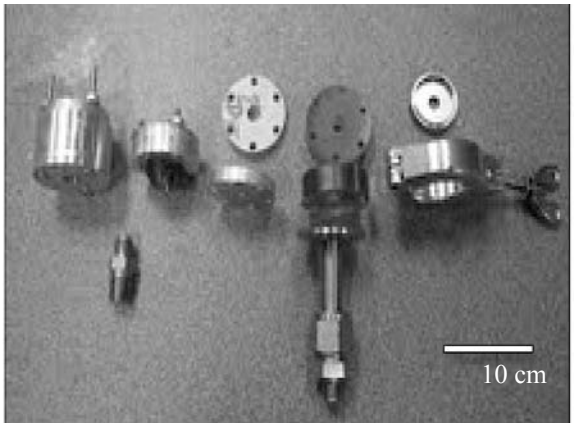

Figure 5.6: Different clamp designs for the bulge tester, starting with a clamp using a sleeve and washers or the right, different clamp designs were made including a ridal clamp (second from the right) and multiple aluminum clamps. The scale bar on the image is 70 cm.

5.4.2. Improving Data Analysis With A Curve Fit

During testing it was also observed that the laser was drifting and was not always and zero displacement when the test began. To properly zero the data a curve fit was made so zero could be found. It was assumed that the pressure and vacuum curves are mirrors of each other. The curve fit used is displayed in Equation 5.1 and the value for are m_1=1, m_2=1, m_3=1 and m_1 is the amount displacement is off by and is added to the displacement values. Figure 5.5 shows the curve fitted data.

$$m_1 * (m_2 - m_1) + m_3 * (m_2 - m_1)^3 \qquad (5.1)$$

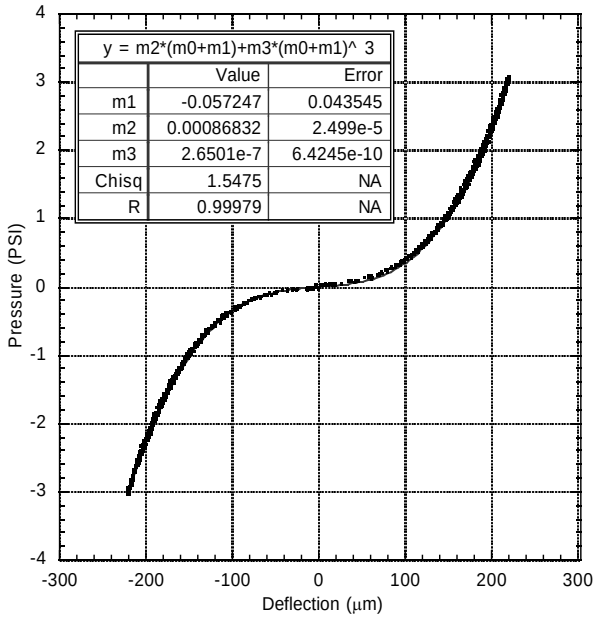

Figure 5.7: This is an example of the curve fitting method used to zero out the bulge test pressure deflection curve for Au/Kapton in the 6 mm Al clamp.

5.4.3. Improving Repeatability of Measurements

After the clamp design was decided on to further improve consistency a x-y microstage was added underneath the clamp set up so the center of membrane could be found accurately every time. To demonstrate the importance of finding the center of the membrane to measure deflection, 100 nm Au 25 μm Kapton were cycled 3 times from 0 to positive 3 psi, at a strain rate of 0.1 psi. Then the using the microstage, the laser was moved 50 μm in the positive and negative x-direction. Figure 5.7 shows deflection is slightly off when were taken from 50 μm off center in the positive and negative x-directions.

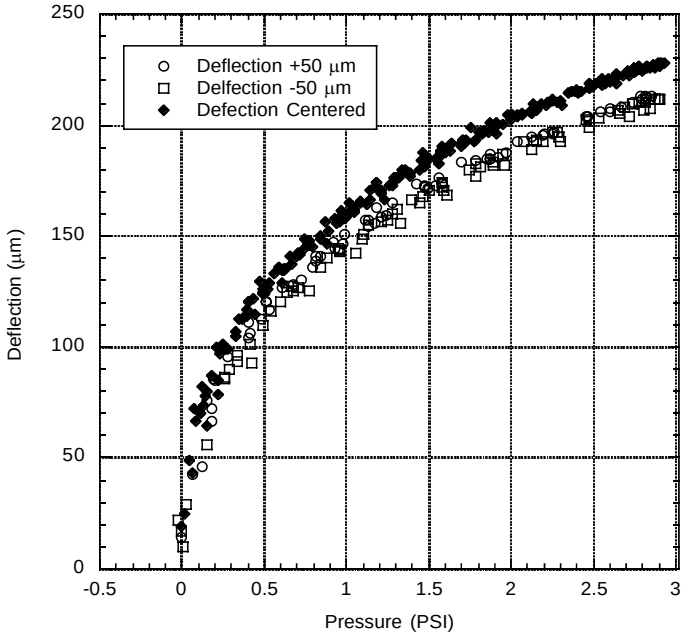

Figure 5.8: Using the x-y stage the measurements were taken at +/- 50 μm off center to show the importance of centering the sample. The sample was 100 nm Au on Kapton with the 6mm Al clamp.

To further identify any variability a torque wrench was used to see if the amount of torque on the screws effected variability. Figure 5.7 shows how the effects of torque on the screws affected the samples. Hand tighten was approximated to be 3 in-lb, the clamp was tightened to 8 in-lbs to see the effects of over tightening the screws. Then samples of 100 nm Au 25 μm Kapton were cycled from positive to negative 3 psi at a strain rate of 0.1 psi.

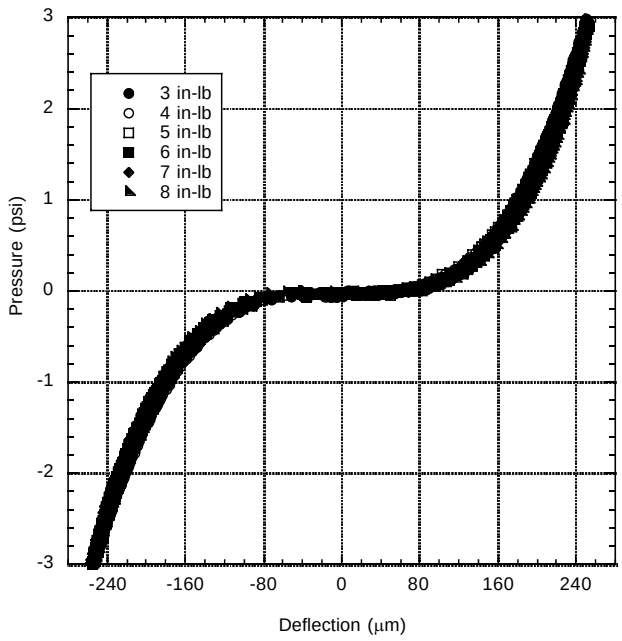

Figure 5.9: The effects of torque on the screws that clamp the sample using Au/Kapton and the 6 mm Al clamp. Torque has little effect on pressure deflection curves.

To minimize slipping, different adhesives were tested to ensure the sample was held properly in the clamp. In order to keep the boundary conditions consistent spray adhesive and super glue was used sparingly on the bottom piece of the clamp up to the hole. Then samples of 100 nm Au 25 μm Kapton were cycled once from positive to negative 3 PSI at a strain rate of 0.1 PSI. Figure 5.8 shows the super glue and adhesive tested using the Au/Kapton samples. The adhesive showed a lot much hysteresis indicating it was compliant. Super glue was rigid enough to hold the sample in place.

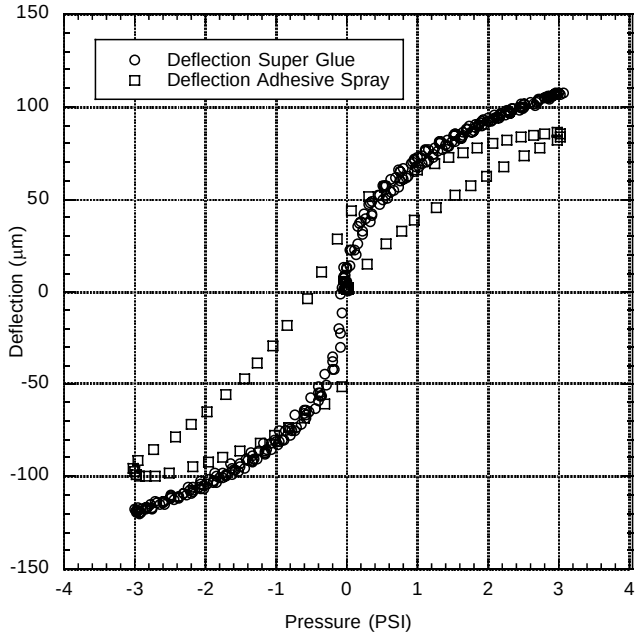

Figure 5.11: Shows the difference in spray adhesive and super glue holding the sample of Au/Kapton in place during testing. Super glue is more effect in holding the sample in place during testing.

After implementing a new clamping system, adding an x-y stage to find an exact zero point, testing the effects of screw tightness, using super glue and a curve fit the data showed no slipping and very little variation and good repeatability as show in Figure 5.10. Using the same samples, maximum pressure and strain rate as the tests above.

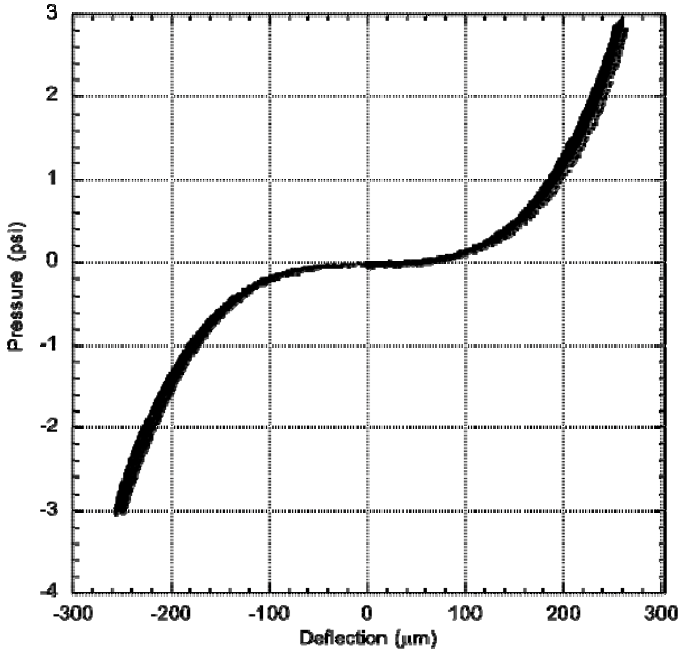

Figure 5.12: 10 different Au on Kapton samples run with the aluminum clamp, super glue and curve fitted to zero. These samples demonstrate the bulge testers ability to take reproducible and repeatable measurements.

5.4.4. Discussion of Improvements of the Bulge Test System

The Clemson University bulge test system shows the importance of design when using a bulge test. The design parameters have been chosen to be used as design guide lines when building a bulge tester for roll-to-roll samples. Testing specimen during roll-to-roll testing it is important to choose a rigid clamping system and using super glue if necessary. It is also important to use consistent torque and to find the exact center of the sample.

5.5. Measurements of Polymer Systems With and Without Heat

An Omega® iSeries CNi8 temperature controller was used to regulate the temperature of 2 ceramic heaters, which provides the heat source. Holes were drilled in the side of the clamp for the ceramic heaters and a thermocouple was place in a hole adjacent to the sample. To set the value to the desired temperature a value is entered into set point 1 through the buttons on the front display. To set the values in the PID loop select configure, then output 1 and PID. Once in the PID menu the rate and cycle can be entered.

The effects of temperature were tested on the micro-fabricated 100 nm Au on 100 nm PMMA on 1 μm SiN_x and the 100 nm Au on 25 μm Kapton. When the samples with 100 nm Au, 100 nm PMMA and 1 um SiN_x were tested with heat, they fractured at 28 °C. This is due to the high residual stress from spin coating PMMA onto a wafer. The rapid solvent evaporation can cause high residual stressed in spin coated polymer thin films [5.19]. The T_g for a 100 nm PMMA film would be expected to be around 80 °C [5.20].

5.5.1. Fabrication and Characterization of Samples Used for Testing With Heat

SiN_x membranes were fabricated at the University of Minnesota Nanotechnology Center to test the reliability of the system. Using a lithography process outlined [5.13], square membranes with a side length of 3 mm were fabricated. The dimensions of the membranes were checked using optical microscopy. Since SiN_x did not have a high reflectivity so the laser cannot be used to accurately measure deflection so gold was used, the 100 nm of Au was deposited onto the SiN_x membranes after fabrication. Figure 5.10

shows a schematic of a fabricated wafer with 12 membranes. In addition, the Au on Kapton systems was examined for temperature effects.

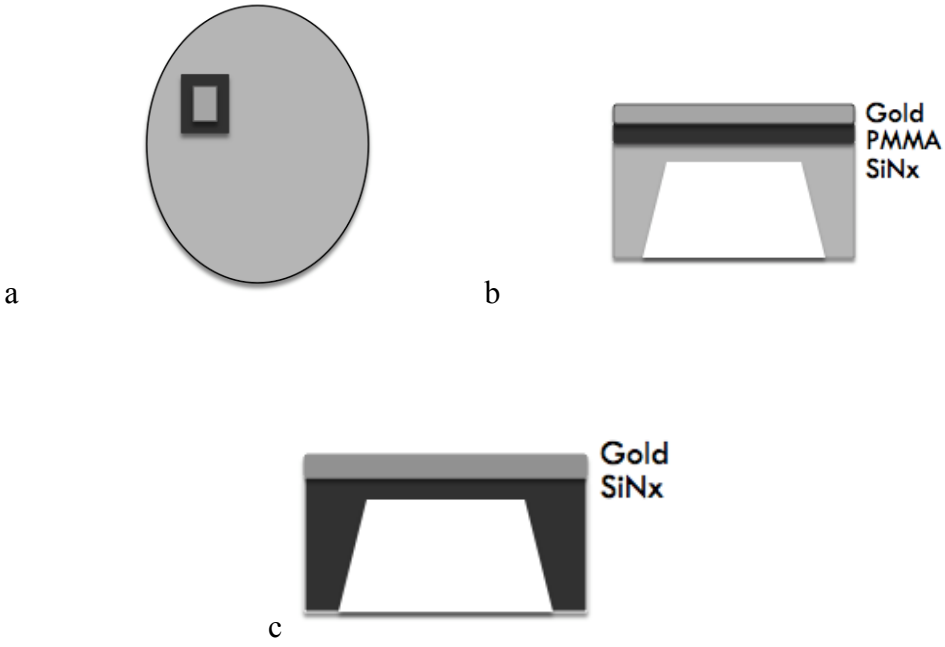

Figure 5.13: (a) a wafer with micro-fabricated dies (b) micro-fabricated dies 100 nm Au on 2 μm SiN_x and (c) 100 nm Au on 100 nm PMMA on 1 μm SiN_x.

5.5.2. Temperature Effects on Au/Kapton Systems

Then samples of 100 nm Au 25 μm Kapton were cycled from positive to negative three PSI at a strain rate of 0.1 psi/s. The pressure deflection curves for the Au on Kapton samples showed no change as temperature increased by 50 °C increments until around 150 °C and a lag in the deformation can be seen. This can be attributed to an increase in diffusion and an increase in polymer chain mobility which dissipates the thermal energy [5.21]. This can be observed in Figure 5.12. The T_g of Kapton is 300 °C.

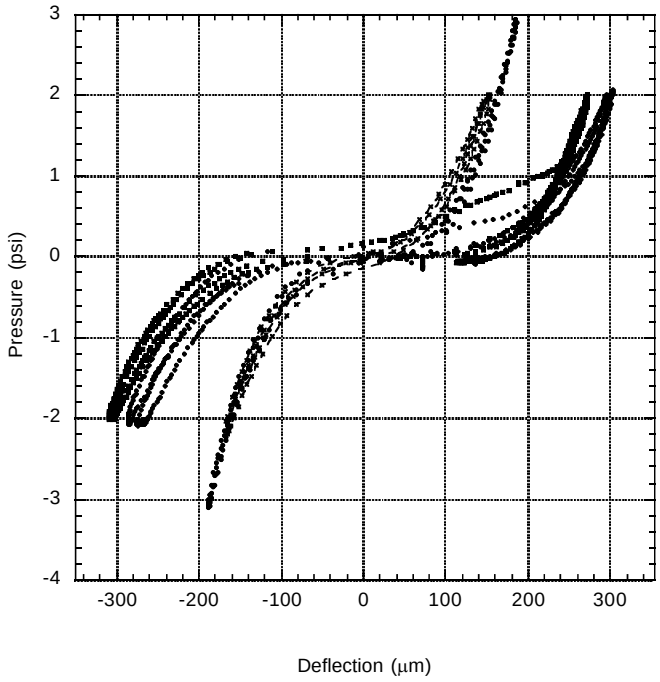

Figure 5.14: As temperature increases past 150 °C, 100 nm Au on 25 μm Kapton shows a lag in deformation in the pressure deflection curve.

5.5.3. Comparison of the Clemson University Bulge Test to Literature

A paper by Huang et al. had similar SiN_x micro-fabricated samples to the ones in this study. Huang's group had 230 nm of SiN_x, with 30 nm Al and samples with 73 nm of PMMA spun onto the same dies. Their data showed an interesting trend that when the polymer film was added to the SiN_x it became harder to deform [5.13]. The pressure deflection is show for their data in Figure 5.13.

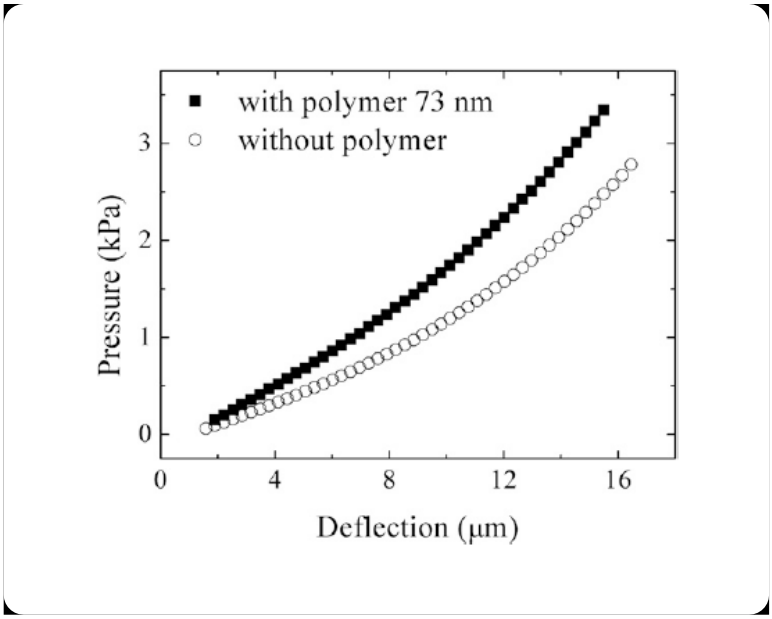

Figure 5.15: Pressure deflection curve for 230 nm SiN_x with 30 nm Al and 73 nm PMMA [5.13]. As a polymer is added the system becomes stiffer, this isn't what would be expected.

5.5.4. Results of SiNx Systems

Samples of 100 nm Au on 100 nm PMMA on 1 μm SiNx were cycled from 0 to 1 PSI at a strain rate of 0.1 PSI/s. The units were converted to kPa so the could be compared to the data from Huang. The Clemson University data showed the same trend as Huang. The sample with spin-coated polymer was stiffer than the sample without. The deflection for the Clemson systems is slightly higher implying that both samples with and without the polymer are more compliant than the samples used by Huang et al. That could be explained by difference in thickness of the samples; the samples used by Haung were thinner than the sample used the residual stresses in the systems are slightly different.

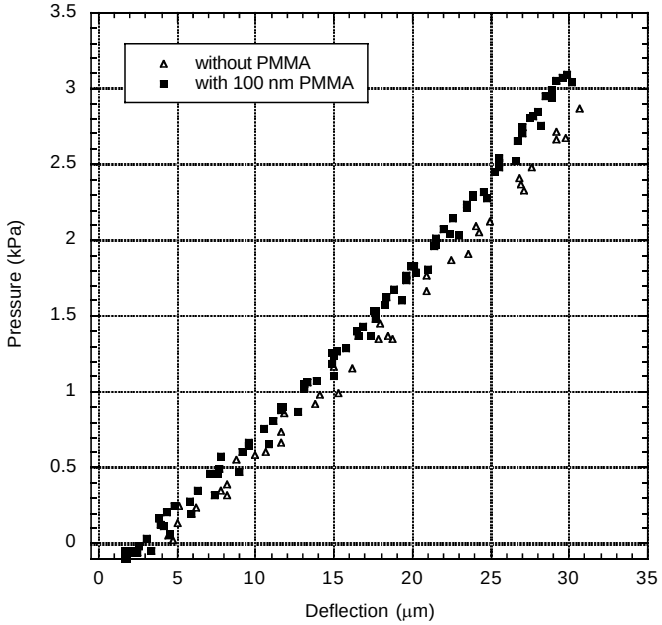

Figure 5.16: Pressure deflection curves for 1 um thick SiNx membranes with the and without PMMA 100 nm. Our membranes showed the same response as Huang's; when a polymer is added the system becomes stiffer.

5.5.5. Temperature Effects on the SiN_x Systems

The effects of heat were also tested on the 100 nm Au on 2 μm of SiN_x. SiN_x has a high melting temperature. We would expect to see very little changes in the deflection of SiN_x as you increase temperature.

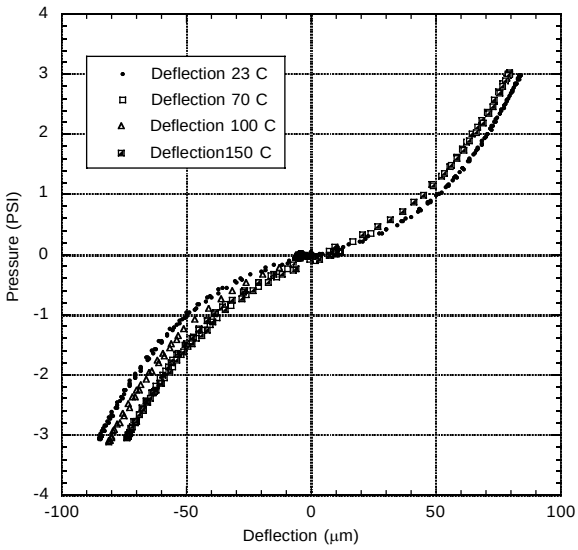

Figure 5.17: 100 nm Au on 2 μm of SiN_x with circular clamp. There is little change in deflection with heat of the SiN_x.

When testing the 100 nm Au, 100 nm PMMA, 1 μm SiN_x, samples with heat the stress in the PMMA as a result of spin coating was so high the sample would fracture without the application of pressure at temperatures above 27 °C.

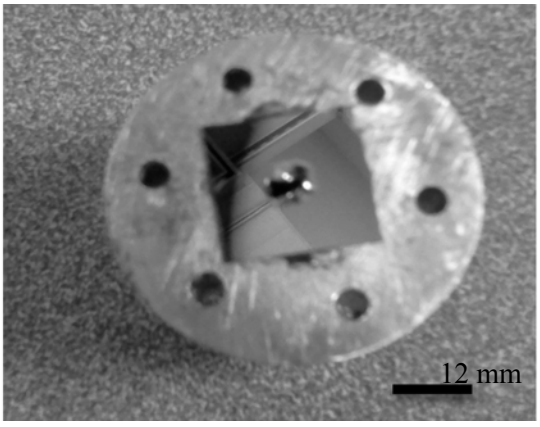

Figure 5.18: 100 nm Au, 100 nm PMMA on 1 μm SiNx that fracture during heating.

5.5.6. Comparing Predicted Values Versus Actual Values of SiN_x Systems

Using the values from Table 5.1 the predicted values for 100 nm Au on 2 μm SiN_x were calculated and plotted against the data from bulge testing using one cycle of positive pressure and graphed in Figure 5.11. The values of the residual stress and biaxial modulus were found using the curve fit (Equation 3.9) and used to predict the response of the Au on SiN_x. The values for the actual data was higher than the predicted values. This can be accounted for by considering residual stress resultant from the processing of the wafers and spin coating the polymer.

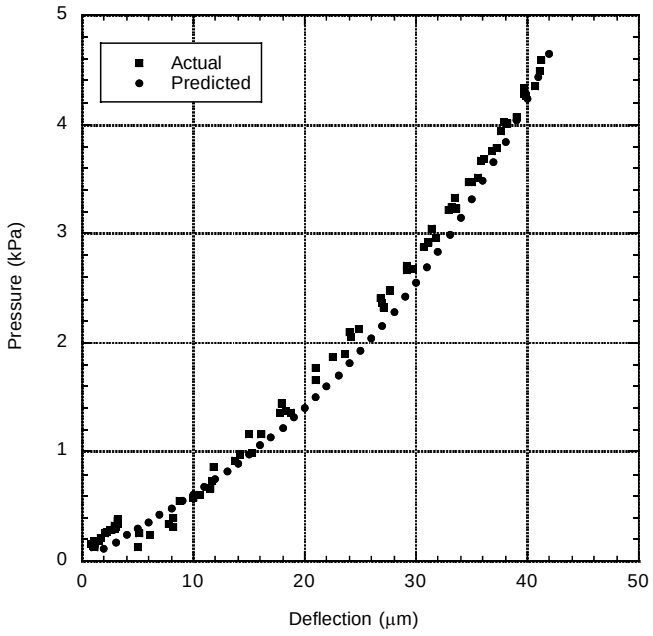

Figure 5.19: Predicted values of 100 Au on 2 μm of SiN_x and actual values using a 6 mm Al clamp. The values are very similar demonstrating the ability of our system to take accurate measurements.

5.5.7. Strain Rate During Bulge Testing

To check the strain rate during bulge testing the 100 nm Au 2 μm SiN_x were pressurized to three PSI and held for approximated 10 minutes. When the film is pressurized and held a sine wave appears in the data. After careful examination it was ruled out this was the temperature controller switching on and off, and determined this is due to environmental conditions (something inside the building).

Disregarding the sine wave general trends can be observed such as when the is done at room temperature there is a relatively straight. Which would be expected as SiN_x is a stiff membrane. However when temperature is applied to the sample the sine wave is amplified and a general trend of relaxation is observed but due to the sine wave it is hard to determine if this actually happening.

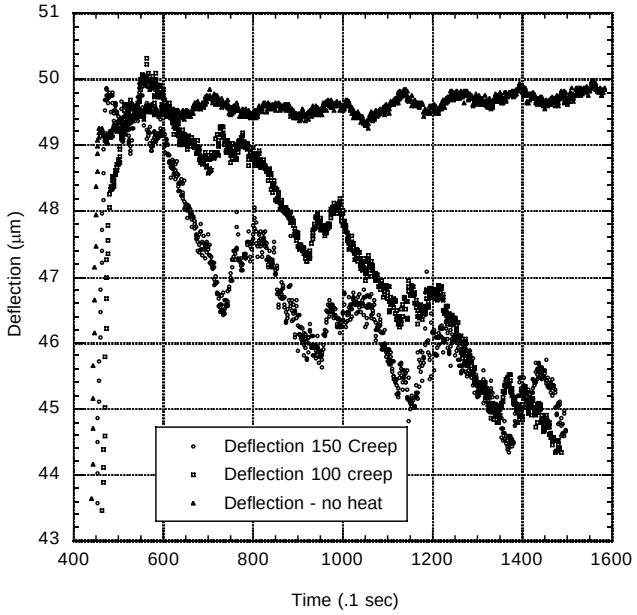

Figure 5.20: The effects of temperature on strain rate during bulge testing, Au/SiNx system using a 6mm Al clamp. A sine wave occurs in the data and makes the data unusable.

5.5.8. Strain Rate Effect With Heat

Using the 100 nm Au on 25 μm of Kapton the strain rate was changed from 0.1 PSI to 2 PSI, and cycled once from +/- three PSI. At low temperature the Au/Kapton system shows very little strain rate sensitivity. When the same system was tested at 200 °C, the pressure-deflection curves show hysteresis, indicating at elevated temperature increases the strain rate sensitivity of Au/Kapton system.

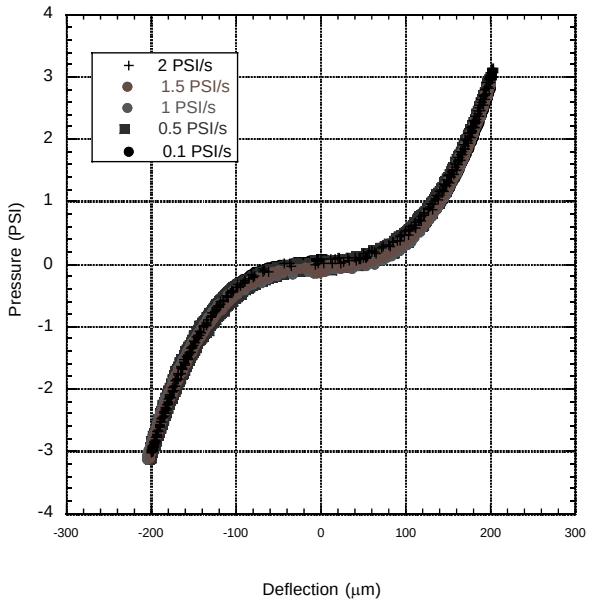

Figure 5.21: By changing the pressurization rate of the bulge tester we are able to see the effect of the strain rate on 100 nm Au on Kapton.

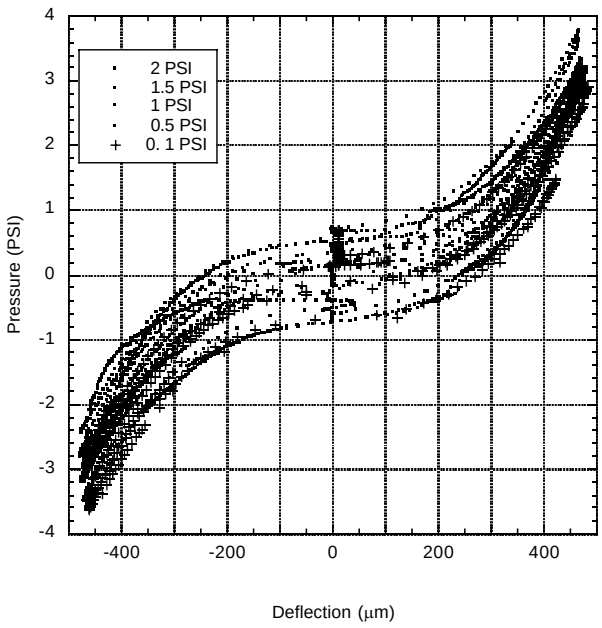

Figure 5.22: Testing the 100 nm Au on Kapton membranes with heat (200 °C) and changing the strain rate we can see that at elevated temperatures polymeric membranes show sensitivity to strain rate.

5.5.9. Discussion of Bulge Testing Polymers With and Without Heat

Little has been done to investigate bulge testing of thin polymer membranes due to their delicate nature [5.22]. Polymer films are commonly spin coated onto silicon wafers and windows are etched into the wafers to try and extract the polymer properties. In order to see a contribution from the polymer it must be as thick as possible or the other material must be as thin as possible [5.13]. The reason the curves look so similar from the samples with and without the PMMA is because the major contribution seen is from the SiN_x. The difference can be accounted for by the increase in residual stress of PMMA fills with decreasing thicknesses. As the T_g is approached the polymer will be come

softer and exhibit a rubbery response to the pressure resulting in less deflection as the energy is dissipated in chain movement and diffusion.

Polymer behavior around the glass transition temperature has been well documented [5.22]. As the polymer gets closer to the T_g it becomes softer and more viscous as shown in Figure 5.21. As a polymer gets thinner the T_g decrease and the effects are seen sooner [5.20]. This behavior is also dependent on the polymer. Studies found PMMA was spin coated on to a silicon wafer the T_g increased from bulk as films thickness decrease due to substrate interaction [5.23]. The same study found that the amount of crystallization and heating rate also effected when the transitional behavior was seen [5.23]. Varying the polymer spin coating solution can control the amount of crystallinity and as the crystallinity increased the deformation response would decrease.

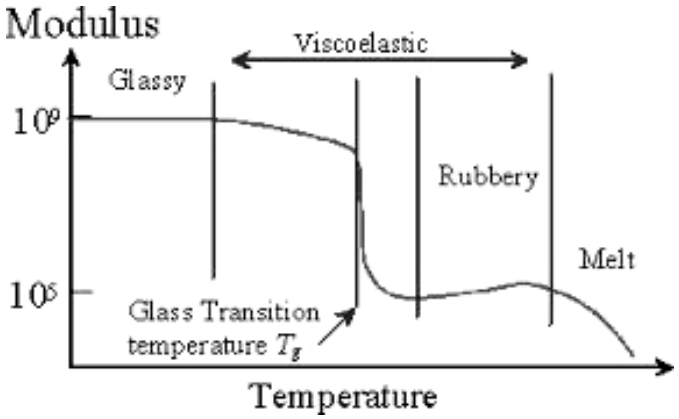

Figure 5.23: Polymer modulus as a function of temperature, as temperature increases the modulus decreases [5.20].

5.6. Conclusions

A bulge tester is a useful tool for extracting composite properties of flexible thin film systems. The Clemson University bulge test system is capable of getting reliable and reproducible results. By designing a new clamping system and super gluing the sample

to the clamp the slipping and variability seen previously were eliminated. Also, by using a lower objective lens and new laser settings the laser is able to stay in focus for larges ranges of deflection (± 500 μm).

The system was then modified to be useful for use in roll-to-roll processing. When using for these applications it is important the system have a proper clamp design. The clamp needs to be stiff enough to be able to keep the sample secure during testing and be able to give reproducible results. We did this by modifying the clamp design, adding a microstage and super gluing the sample to the clamp.

By adding a heater the bulge test system is capable of measuring materials properties over a wide range of temperatures (up 200 °C). If a system has a T_g within the range of the heater it would be possible to see the effects of the T_g on system behavior.

5.7. References

[5.1] M. Small and W. D. Nix, "Anaylsis of the accuracy of the bulge test in determining the mechanical properties of thin films," Journal of Material Research, vol. 7, pp. 1553-1563, 1992.

[5.2] T. Tsakalakos, "The Bulge Test: A Comparison Of Theory And Experiment For Isotropic And Anisotropic Films," Thin Solid Films, vol. 75, pp. 293-305, 1981.

[5.3] Y. Xiang, et al., "The Mechanical Properites of Electroplated Cu Thin Films Measured by means of Bulge Test Techniques " Material Research Society, vol. 695, pp. L4.9 1-6, 2002.

[5.4] H. Keiner, et al., "Avanced Bulge Test System," Material Research Society, vol. 505, pp. 229-234, 1998.

[5.5] A. Nakladal, et al., "Bulge Test Investigation of the Influence of Moisture on Mechanical Properties of Thin Polymer Layers " Material Research Society, vol. 518, pp. 2378-2382, 1998.

[5.6] X. Wei, et al., "Plane-strain bulge test for nanocrystalline copper films," Scripta Materialia, vol. 57, pp. 541-544, 2007.

[5.7] Y. Xiang, et al., "High ductility of metal film adherent on a polymer substrate," Applied Physics Letters, vol. 86, 2005.

[5.8] R. Edwards, et al., "Comparison of Tensile and Bulge Testing for Thin-Film Silicon Nitride," Society for Experimental Mechanics, vol. 12, 2003.

[5.9] J. Mitchell, et al., "Examination of Bulge Testing for Determining Residual Stresses, Young's Modulus, and Poissions Ratio of 3C-SiC Thin Films," Journal of Aerospace Engineering, vol. 46, pp. 46-55, 2003.

[5.10] M. Kennedy, et al., "Coupling bulge testing and nanoindentation to characterize materials properties of bulk micromachined structures," Microsystem Technologes, vol. 11, pp. 782-797, 2005.

[5.11] T. Tsakakos, "The Bulge Test: A Comparison of Theory and Experiment for Isotropic and Anisotropic Films," Thin Solid Films, vol. 75, pp. 293-305, 1980.

[5.12] T. Tsakalakos, "Elastic modulus in compostiton-modulated copper-nickel foils," Journal of Applied Physics, vol. 54, pp. 734-738, 2001.

[5.13] C. K. Huang, et al., "Mechanical Properties of polymer thin film measured by bulge test," Thin Solid Films, vol. 515, pp. 7222-7226, 2007.

[5.14] F. Maseeh and S. D. Senturia, "Viscoelasticity and Creep Recovery of Polymide Thin Films," IEEE, vol. 90, pp. 1348-1356, 1990.

[5.15] A. J. Kalkman, et al., "High-Temperature bulge test setup for mechanical testing of free-standing thin film," Review of Sciencetific Instruments vol. 74, pp. 1383-1385, 2003.

[5.16] B. E. Alaca and K. B. Toga, "Strain-Controlled Bulge Test," Journal of Material Research , vol. 23, pp. 3295-3302, 2008.

[5.17] K. Gavan, et al., "Size-dependent effective Young's Modulus of silicon nitride cantilevers," Applied Physics Letters, pp. 389-420, vol. 94, 2009.

[5.18] M. C. Salvadori, et al., "Measurement of the elastic modulus of nanostrucuted gold and platinum thin films," Physical Review B, pp. 5793-5801, vol. 67, 2003.

[5.19] D. Hall, et al., "Spin Coating Thin and Ultrathin Polymer Films," Polymer Engineering and Science, vol. 38, pp. 2039-2044, 1998.

[5.20] J. Zhao, et al., "Thermal stess and glass transition temperatue or ultrathin polystyrene films," Applied Physics Letters, vol. 77, pp. 2843-2845, 2000.

[5.21] K. C. Tseng, et al., "Molecular mobility in polymer thin films," Physical Review E, vol. 61, pp. 1800-1811, pp. 345-354 2000.

[5.22] J. Torres, et al., "Molecular Simulation of Ultrathin Polymeric Films Near the Glass Transition " Physical Review Letters, vol. 85, pp. 3221-3324, 2000.

[5.23] C. Porter and F. Blum, "Thermal Characterization of PMMA Thin Films Using Modulated Differential Scanning Calorimetry," Macromolecules, vol. 33, pp. 7016-7020, 2000.

CHAPTER SIX

FUTURE WORK

6.1. Contributions From This Work

Flexible electronic systems have the potential to be used in many aeronautic applications. Poor adhesion in these systems can lead to compressive driven buckling or tensile driven cracking and can causes device failure. This work used metal-polymer thin film systems to show film thickness, interlayer chemistry and substrate type can chance the system's reliability under tensile and compressive stress. In addition, this thesis also outlines the creation of a heating element for a bulge test system and a new sample preparation method for roll-to-roll samples.

A combitorial film system was fabricated at Sandia National Laboratories using W films were deposited onto PMMA and PS. By altering the film stress, interlayer composition (substrates with and without aluminum oxide interlayers) and substrates, a range of failure mechanisms were observed including both tensile buckling and tensile cracking. The fracture energy was estimated by using previous work by Hutchinson and Sou . It was found that the for tensile driven deadhesion for W on PS it was found that as film thickness increases the energy release rate increases (0.002 J/m^2 to 0.01 J/m^2). With the inclusion of an interlayer, which changed the chemistry and the interface, the interfacial fracture energy decreased by an order of magnitude (0.001 J/m^2 to 0.03 J/m^2) but still showed increasing film thickness, increased the energy need for delamination. Using compressive W on PMMA, the same trends were observed, an increase in energy

release rate with an increase in film thickness. An additional trend of two different sizes of buckle (small and large) was observed on the 400 and 600 nm films. The compressive films without an interlayer were up to 3 orders of magnitude larger than the tensile films (0.8 J/m^2 to 2.4 J/m^2) and the interlayer only slightly increase the energy release rate (0.4 J/m^2 to 2.8 J/m^2) for the compressive films.

Many models have been presented to explain the deformation behavior of metallic films on rigid substrates, however, few have taken into account the compliance of the substrate. When the film is buckled, it deforms the substrate as shown in Chapter 4 using compressive W on PMMA. In this Chapter, we also define the d:b zone (ratio of buckle width to the width of the deformation zone), which quantifies the amount of deformation seen in the substrate.

A bulge tester has been modified for roll-to-roll specimens and to test at elevated temperatures (23 °C to 200 °C). The bulge test system was optimized for flexible systems by paying special attention to the specifics of bulge testing such as laser readings, clamping conditions and temperature settings. It was also shown to take reproducible results as demonstrated by comparing the measurements to literature values and predicted values.

6.2. Future Work

This work has helped confirm evidence of substrate deformation and show bulge testing can be used in industrial applications. Although these contributions to the work done on flexible films systems are a positive step in the right direction more work still needs to be done. Three areas that should be explored in the future are: (1) find a way to

isolate the noise seen in the bulge test system during creep tests, (2) use the bulge tester to verify the effects of film thickness on T_g and (3) use the AFM to measure changes in hardness or phase throughout the deformation zones.

6.3. Isolating Noise Seen in the Bulge Tester

In Chapter 5, a 100 nm Au on 25 μm Kapton membrane was heated to room temperature, 100 °C, 150 °C and held for 10 minutes. This load displacement in the center of the round membrane showed an unexpected sinusoidal decay. This decay might be due to the a reasonance from a generator within the building. Need to explain the change in temperature.

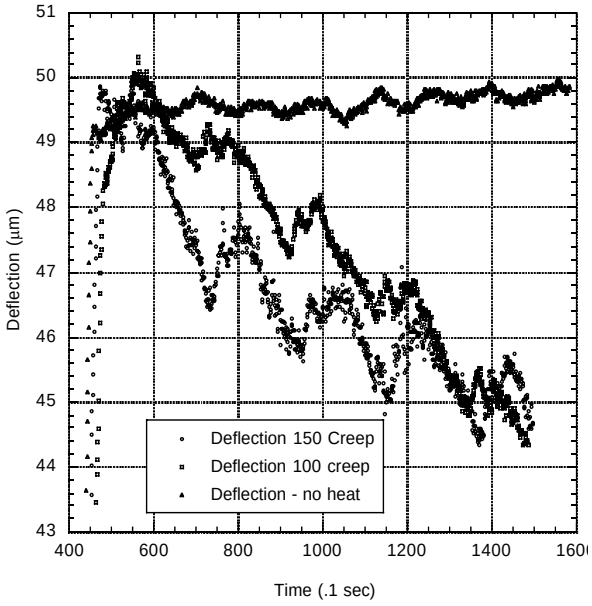

Figure 6.1: the results of holding Au/Kapton at various temperatures, no trends can be seen due to interference.

6.4. Use the Heated Bulge Test to Verify How Film Thickness Effects Tg

The glass transition temperature of a polymer thin film has been shown to be a function of the film thickness [6.2]. This was demonstrate by using differential scanning calorimtry [6.3]. To determine if this could be seen using the bulge tester, films of decreasing thickness could be tested at heat increments of 10 °C until a change in the pressure-deflection curve is seen. As the film approaches the T_g, deflection of the membrane will continue to decrease until an abnormal or undistinguishable curve is produced.

6.5. Use the AFM to Map d:b Zones

The AFM can be used in noncontact mode [6.4], or pulse force mode [6.5] to measure polymer surfaces [6.4] and nano-structured materials [6.5]. By using force-distance curves to measure the interaction of the tip with the sample, and indentations to measure hardness we can being to map out adhesion [6.5], stiffness [6.5] and hardness [6.4] of the deformation zones in compliant substrates. d:b ratios give a good idea of substrate deformation but mapping out adhesion and stiffness will give a better idea of how flexible substrates deform.

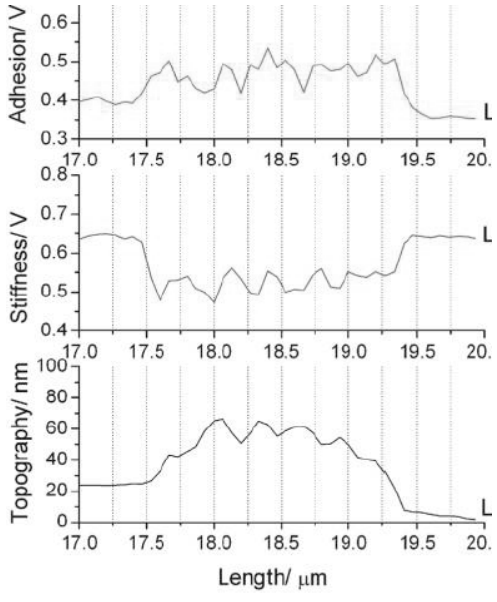

Figure 6.2: Adhesion, Stiffness and topography version length graphs of PINPAM polymer thin film surface.

6.6. References

[1] F. Maseeh and S. D. Senturia, "Viscoelasticity and Creep Recovery of Polymide Thin Films," IEEE, vol. 90, 1990.

[6.2] J. Torres, et al., "Molecular Simulation of Ultrathin Polymeric Films Near the Glass Transition " Physical Review Letters, vol. 85, pp. 3221-3324, 2000.

[6.3] K. C. Tseng, et al., "Molecular mobility in polymer thin films," Physical Review E, vol. 61, 1999.

[6.4] J. W. Hutchinson and Z. Sou, "Mixed mode cracking in layered materials," Advances in applied mechanics, vol. 29, pp. 63-191, 1992.

[6.5] B. Lui, et al., "Low tip damage AFM technique developmet for nano structures characterization," Journal of Applied Physics, vol. 77, 2010.

[6.5] C. Rezende and L.-T. Lee, "Surface Mechanical Properties of Thin Polymer Films Investigate by AFM in Pulse Force Mode," Physical Review Letters, vol. 25, pp. 9938-9946, 2009.

APPENDICES

Appendix A: Operation of the Clemson University Bulge Test System

A.1. Set-up of System

1. Turn on the MSA 400 System by turn the key on the bottom computer to on, and the switch the middle computer on
2. Make sure the Nitrogen gas cylinder is open to at least 3 psi
3. Turn on the vacuum pump located behind the MSA computer rack
4. Turn on the pressure controller
5. Turn on the power supply for the pressure transducer
6. Once the MSA 400 computer is on select the measurement program from the desk top
7. In the software on the right tool bar there is a box that says laser select that box. Note: it takes 15-30 minutes for the laser to warm up

A.2. Sample Prep

1. Unscrew the aluminum clamp from the system and take apart the clamp
2. To prepare a flat specimen it is help full to use the silicon mat laying to the right of the MSA 400 on the pressure table.
3. Put the sample face down on the mat and smooth out all air bubbles or wrinkles
4. On the bottom half of the clamp, the thicker section, put a small amount of super glue and spread evenly around the hole
5. Next lay the bottom half of the clamp on top of the sample on the silicon mat and let it dry for 1-2 minutes
6. Slowly remove the sample and clamp from the mat
7. Next screw the top half of the clamp, the thinner section, on top of sample and screw on the nuts until they are flush with the clamp

A.3. To Begin Testing

1. Screw the clamp in the holder
2. Focus the laser using the coarse and fine adjustment knobs on the side of the MSA 400

3. To center the laser find the edge of the clamp by moving the knobs on the x-y stage and center horizontally, then using the x move 5 full turns to the center of the sample.

4. If laser signal is low try turning the fine adjustment know to strengthen it or use the knob where the laser head feeds into the MSA 400.

5. Open LabView on the Dell desktop computer

6. Select the VI Nathan Try

7. To begin the program push the white arrow at the top

8. If the displacement is not zero, plug in the displacement cable into the bottom MSA computer on the terminal on the left labeled displacement and select the reset button on the VI

9. Next in the drop down menu labeled d.p. (decimal points) select 4 d.p.

10. In the menu labeled units select PSI

11. If you wish to change the pressure rate you may do so in the menu labeled pressure rate, it is normally left at MAX and Rate is 1. This can be changed to control the strain rate.

12. In the box labeled set point enter the desired pressure ie 3

13. To begin controlling pressure hit control and change in the underneath the setpoint

14. Once the test is running you must control the pressure manually, so once the pressure value (3) is reached you must enter the minimum value -3. Negative values correspond to vacuum. *If the vacuum pump is not on the pressure won't go below 0.

15. Cycle the pressure as desired

16. Once the test is over to end the test click control, then quit and then stop acquisition

17. The test will be exported as a data file in documents, Labview Data. Scroll down to test 1 and open it. The do a file save as txt and save the date your folder.

18. The data that is exported in the following order: time (.1s), pressure (units you selected), and displacement (μm).

19. If at anytime the test needs to be stopped (control, quit, stop acquisition) there is a vent button to release the accumulated pressure. The vi must be running for the vent button to work.

A.4. Important Features of the VI Interface

1. There is a reading of the laser strength on the vi it should be maximized
2. There are multiple graphs displaying pressure and deflection, pressure and time and deflection and time.
3. There is also a gauge that reads the pressure transducer value, the read out at the top is the pressure controller value

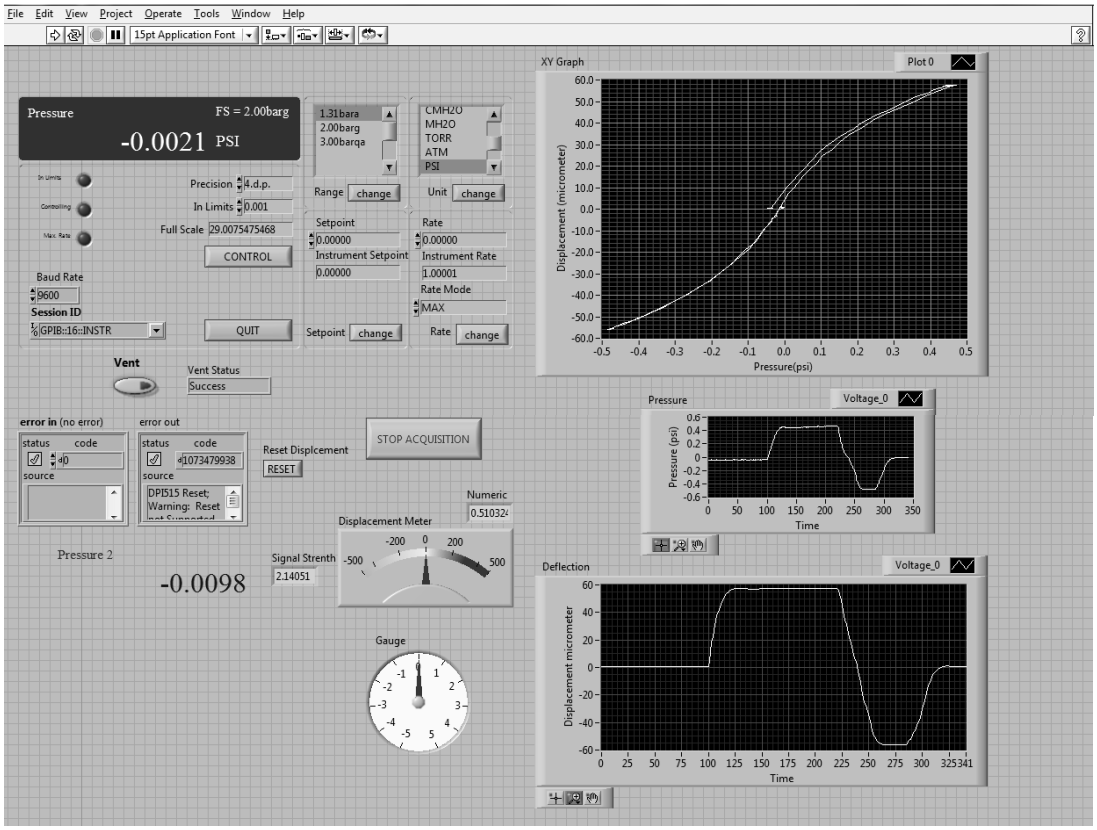

Figure A.1: Screen shot of the VI interface and important features such as the system pressure, pressurization rate, set point and deflection of the sample.

APPENDIX B

BLOCK DIAGRAMS OF BULGE TEST VIRTUAL INTERFACE

The block diagram for the VI program Nathantry.vi, a program designed by Nathan Mitchell, is set up into two loops. The first loop controls the pressure controller and the design was provided General Electric on their website for using the DPI pressure controller. This loop gives the operator the ability to input the precision (decimal places), pressure rate, range, units of pressure and set point can be seen as input values. Also the vent function, which vents any pressure or vacuum, is controlled in this loop, designed by Nathan Mitchell. This loop does not write to file as all pressure values are taken from the pressure transducer. This loop is shown in Figure B.1. It regulates pressure at the given set point and changes the pressure at the rate specified by the user.

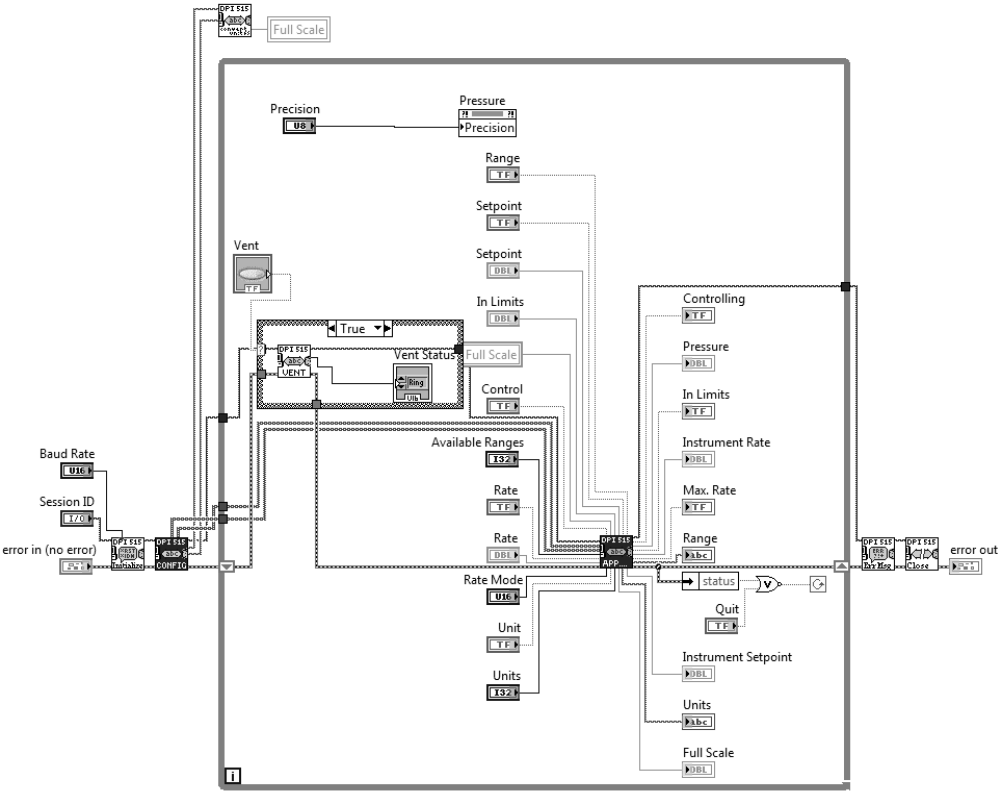

Figure B.1: The loop that tells the pressure controller pressurization rate and set point the block diagram for the bulge tester.

In the second loop (as seen in Figure B.2) three data channels are collected from a DAQ, it runs 10 loops a second. The first channel is from the laser vibrometer displacement output. This channel comes out and splits into three parts the first part is multiplied by 50 μm per volt, this value was determined in the laser vibrometer program as having the best resolution and must match the value set in the vibrometer settings. After this conversion a displacement value is displayed as a meter and numeric value. The second line splits is feed through a build array and pass node where it is then multiplied by 50 μm per volt and is the y input in the deflection over time graph. The third split of displacement line goes to a build array and pass node is written to file as a

displacement value in μm.

The second channel is from the pressure transducer, it is also split into different nodes, but first is multiplied by 8.9014 which converts the voltage signal into a pressure value in PSI and then offset by 14, a correction value, which set the pressure value to zero. After these linear fits, the line splits; first it display instantaneous pressure as a gauge value. The second split goes through a build array and pass node where it is the x input in pressure graph display.

The last channel input is the laser signal strength, which is read as a voltage and displayed as a numerical value. When focusing the laser, trying to get this value as high as possible will lead to better laser focus. Other features are the displacement offset. This re-zeros the displacement. The text file is written as three columns in this order: time (in .1 seconds), pressure in PSI and displacement in μm.

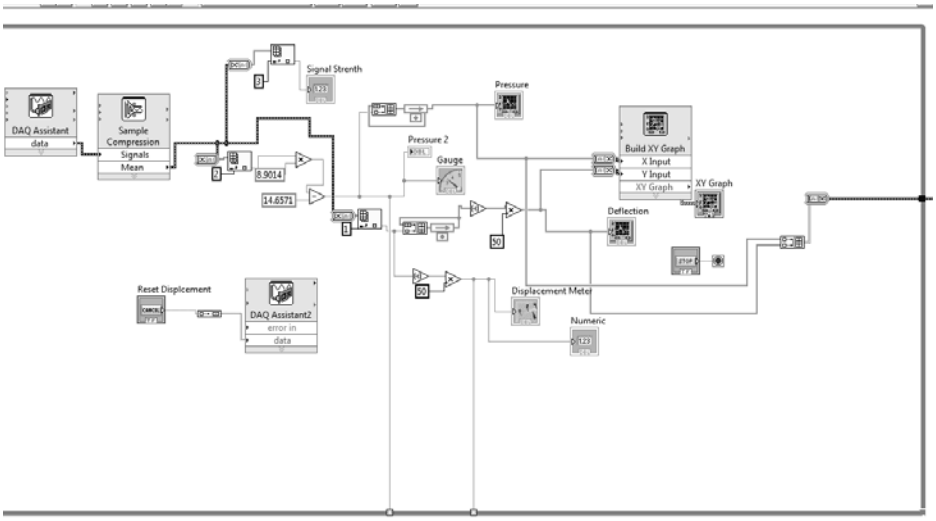

Figure B.2: The second loop of the block diagram that controls the pressure transducer, displacement and laser signal.